People's Democratic Republic of Algeria

Ministry of Higher Education and Scientific Research

N°:……..

University Mohamed Boudiaf of M'Sila

Faculty of Technology

Department of Electronics

A Dissertation Submitted in Partial Fulfillment of

the Requirements for the Degree of Master in

Telecommunications Systems

Analysis of Some CFAR Processors for High-Resolution Radar Systems

Submitted by:
- Abir DAIRA
- Fadwa BENMEBAREK

Supervised by:
Dr. Mohamed SAHED
Dr. Elhadi KENANE

Defended on June 20, 2023 in front of the following board of examiners:

Ali KHALFA	MCA	University of M'Sila	Chairman
Mohamed SAHED	MCA	University of M'Sila	Supervisor
Elhadi KENANE	MCA	University of M'Sila	Co-supervisor
Izzedine CHALABI	MCA	University of M'Sila	Examiner

Academic Year: 2022/2023


بسم الله الرحمن الرحيم

Dedications

To my dear mother

No matter what I do or say, I'll never be able to thank you properly. Your affection covers me, your mercy guides me and your presence by my side has always been my source of strength to face various obstacles.

To dear Father

You have always been by my side to support and encourage me. I hope this work reflects my gratitude and affection.

To my dear brothers

Faiz, Thabet, Tarik, Sebti,

To my gift my beautiful sisters: Siham and Randa

To all the members of my extended family Daira and Baadji.

Special thanks to Professor Brik Youcef

To my colleagues to all those who have contributed in any way even though simple advice, to ensure that this research work produced convincing results. May God grant your health, happiness, courage and above all success.

Abir

Dedications

First of all, I want to thank ***ALLAH***

For giving me the strength and the courage to lead good at this modest job.

I would like to dedicate this humble work to:

My dear mother

You are the heroine of my life, you are my role model, you are the reason for my success and excellence. Thank you for your constant support, mom.

To my dear father

Thank you, ***ALLAH***, for choosing me and blessing me to be my father, to belong to this beauty all my life.

Thank you, father, for your fear, your concern, and the doses of optimism that you used to water me with your words. May God prolong your life and protect you for me, O Lord.

To my dear brothers Hicham and Mohamed

I thank you, my brothers, for your continued support for me and for helping me in the affairs of my life.

To all my family and friends. To my partner Abir and to the entire Ben Mebarek family and Mokhtari. And to everyone who directly or indirectly contributed to making this project possible, I say thank you.

I also extend my sincere thanks to the professors of the Department of Electronics, especially Professor Mahroug, Professor Kinan Al-Hadi, and the supervisor Professor, Sahed Mohamed

Fadwa

Acknowledgement

*Above all, our thanks go to **Allah** the **Almighty** for giving us the health, strength and patience to accomplish this modest work ... without **Him** nothing is done or created.*

First, we would like to thank our parents for their moral support and encouragement.

We would like also to warmly thank our supervisor Dr. Mohamed SAHED and co-supervisor to Dr. Elhadi KENANE for their guidance, support and advice, and their invaluable comments, which enabled us to overcome the difficulties and make progress in this study.

Our sincere thanks also go to Dr. Ali KHALFA, for the honor he bestowed on us by agreeing to chair the jury examining this dissertation.

We would also like to express our sincere gratitude to Dr. Izzedine CHALABI for accepting the role of examiner on the jury and for the time he devoted to reading this manuscript.

Special thanks go to all the teachers in the Electronics Department at the University of M'Sila.

We are fully aware that short comings and mistakes are inevitable in we research. Any comments and suggestions would be highly appreciated for the perfect of we own research.

D.Abir

B.Fadwa

Abstract

In this study, we address the problem of adaptive detection of embedded radar targets in a Pareto distributed clutter. This type of detection is achieved by maintaining a constant false positive rate (CFR) during processing. We first introduce the geometric mean CFAR (GM-CFAR) detector introduced in the literature. The detector is suitable for homogeneous clutter. We show that the derivation of this detector is obtained by exploiting the duality between both exponential and Pareto distributions. This duality makes it possible to convert CFAR detection strategies developed for Gaussian noise into Pareto distributed clutter. In addition, we have presented a modified version of the GM-CFAR, which is called the Maximum Likelihood (ML) CFAR detector, and thus give the corresponding analytical expression of the false alarm probability. For comparison purposes, we perform as well a partial theoretical analysis of two other detectors, namely the Greatest Of (GO) CFAR and the Smallest Of (SO) CFAR algorithms. Via numerical simulations, the performance of the ML-CFAR scheme has been compared and examined against those of the Optimal, GM, GO and SO-CFAR detectors. The simulation results obtained validate the interest of the ML-CAFR detector in homogenous backgrounds, but shows that its performance degrades in heterogenous backgrounds. Moreover, it has been also shown from these results that the SO-CFAR detector is relatively efficient against interfering targets.

Keywords: Radar CFAR detection, non-Gaussian clutter, Pareto-Distribution, Maximum Likelihood Estimates, ML-CFAR, GM-CFAR, GO-CFAR, SO-CFAR.

Tables of Contents

List of Symbols and Notations ..... **iv**
List of Figures ..... **vi**
Introduction **1**
A. Preamble 2
B. Historical Background 2
C. Motivations 3
D. State of the Art 4
E. Organization of the Dissertation 5
Chapiter 1 : Basics of Radar Signal Detection in Noise **7**
1.1 Introduction 8
1.2 Binary Detection theory 8
1.3 Radar Signal Modeling 9
1.3.1 Clutter modeling 9
1.3.2 Target Modeling 14
1.4 Optimal Neyman-Pearson detector 17
1.5 CFAR Detection 18
1.5.1 Formulation of the CFAR detection problem 18
1.5.2 Principle of CFAR detectors 19
1.5.3 Decision rule in a CFAR detector 19
1.6 Conclusion 21
Chapiter 2 : CFAR Detection in Homogenous Pareto-Distributed Clutter **22**
2.1 Introduction 23
2.2 Statistics of the CUT 23
2.2.1 CUT's Statistics under $\boldsymbol{H0}$ 24
2.2.2 CUT's Statistics under $\boldsymbol{H1}$ 24
2.3 Optimal fixed threshold detector 26
2.3.1 P_{fa} of the optimal fixed threshold detector 27
2.3.2 P_d of the optimal fixed threshold detector 28
2.4 Geometric Mean (GM) CFAR detector 28
2.5 Maximum Likelihood (ML) CFAR detector 33

2.5 Greatest of (GO) CFAR detector 37
2.6 Smallest of (SO) CFAR detector..... 39
2.7 Conclusion 41
Chapiter 3 : Simulation Results 42
3.1 Introduction..... 43
3.2 Simulation parameters..... 43
3.3 Comparison between ML- CFAR and GM-CFAR 44
3.4 Analysis of detection performance in homogenous backgrounds..... 47
3.5 Analysis of detection performance in heterogenous backgrounds..... 49
3.5.1 Case 1: Presence of a single interfering target..... 49
3.5.2 Case 2: Presence of more than one interfering targets..... 52
3.5 Conclusion 54
Conclusion and perspectives 55
References 57

List of Acronyms

RADAR	Radio Detection and Ranging
UE	Unbiased Estimator
IEEE	The Institute of Electrical and Electronics Engineers
ITU	The International Telecommunication Union
FAR	False Alarm Rate
CFAR	Constant False Alarm Rate
CUT	Cell Under Test
SNR	Signal-to-Noise Ratio
SCR	Signal-to-Clutter Ratio
ICR	Interference-to-Clutter Ratio
iid	Independent and identically distributed
r.v.	Random Variable
PDF	Probability density function
CDF	Cumulative distribution function
RF	Radio Frequency
EM	Electromagnetic
PPI	Plan Position Indicator
CW	Continuous-Wave,
RCS	Radar Cross Section
MLE	Maximum Likelihood Estimator
CA-CFAR	Cell Averaging CFAR
GO-CFAR	Greatest Of Selection Logic in Cell Averaging CFAR
SO-CFAR	Smallest Of Selection Logic in Cell Averaging CFAR

List of Symbols and Notations

$Pa(\alpha, \beta)$	Pareto distribution with parameters α and β.
$Exp(\mu)$	Exponential distribution with mean parameter μ.
$p_X = 2\sigma_X^2$	Mean Power of Clutter echo X
$p_Y = 2\sigma_Y^2$	Mean Power of target signal Y
μ	Arithmetic Mean
σ	Standard Deviation
σ^2	Variance
c	Shape parameter of the Weibull distribution
b	Scale parameter of the Weibull distribution or the *K* distribution
ν	Shape parameter of the *K* distribution
α	Shape parameter of the Gamma distribution
β	Scale parameter of the Gamma distribution
I_c	In-phase component of the received signal
Q_c	In-Quadrature component of the received signal
H_0	Null hypothesis of detection test that indicates target is absent
H_1	Alternative hypothesis of detection test that indicates target is present
Y	Signal utile de la cible
X	Clutter (ou échos parasites)
ϕ	Random Angle between X et Y
Z	Sufficient Statistic Test
Z_0	Signal in the CUT
N	Number of cells (observations) in one half of the reference window of a CFAR detector
$2N$	Number of cells (observations) in the reference window of a CFAR detector
P_d	Probability of Detection
P_{fa}	Probability of False Alarm
α_0	Desired Probability of False Alarm
X	Random variable
x	Particular observation of the random variable X
$f_X(x)$	Probability density function, PDF
$F_X(x)$	Cumulative Distribution Fonction, CDF

$f_{X\|Y}(x\|y)$	Conditional Probability density function of X given Y
$f_{Z_0}(z_0\|H_i)$	Conditional PDF of X under hypothesis H_i, $i = 1$ or 2.
$F_{Z_0}(z_0\|H_i)$	Conditional CDF of X under hypothesis H_i, $i = 1$ or 2.
T	Multiplication (or Scaling) Factor of a CFAR detector
λ_{CA}	Detection threshold of the CA-CFAR detector
λ_{GO}	Detection threshold of the GO-CFAR detector
λ_{SO}	Detection threshold of the SO-CFAR detector
$\Gamma(\cdot)$	Gamma Function of Euler
$K_v(\cdot)$	Modified Bessel Function of the second kind of order v
$\binom{k}{n}$	Binomial Coefficients $= \frac{k!}{n!(k-n)!}$ with $n \leq k$
dB	Decibel
GHz	Giga Hertz

List of Figures

Figure 1.1 - Probability density function of the Gaussian law (①μ=0 ②σ=1)..... 10
Figure 1.2 - Probability density function of Rayleigh distribution 11
Figure 1.3 - Probability density function of the Lognormal distribution 11
Figure 1.4 - Probability density function of the Weibull distribution 12
Figure 1.5 - Probability density function of the *K* distribution 13
Figure 1.6 - Probability density function of the Pareto distribution..... 14
Figure 1.7 - Swerling Model I..... 15
Figure 1.8 - Swerling Model II..... 16
Figure 1.9 - Swerling Model III 16
Figure 1.10 - Swerling Model IV 17
Figure 1.11 - Optimum Neyman-Pearson detector 18
Figure 1.12 - Block diagram of a CFAR adaptive detector..... 21
Figure 2.1 - Block diagram of the GM-CFAR detector 32
Figure 2.2 - Block diagram of the ML-CFAR detector..... 36
Figure 2.3 - Block diagram of the GO-CFAR detector..... 39
Figure 2.4 - Block diagram of the SO-CFAR detector..... 41
Figure 3.1 - Impact of variation of the value of the shape parameter α on the detection performance of the GM-CFAR and ML-CFAR detectors for $M = 16$ and $\alpha 0 = 10 - 4$..... 46
Figure 3.2 - Impact of variation of the length M of the reference window on the detection performance of the GM-CFAR and ML-CFAR detectors for $\alpha = 4.7241$ and $\alpha 0 = 10 - 4$. 46
Figure 3.3 - Impact of variation of the desired false alarm probability $\alpha 0$ on the detection performance of the GM-CFAR and ML-CFAR detectors for $\alpha = 4.7241$ and $M = 16$..... 47
Figure 3.4 - Probability of Detection of Optimal, ML-CFAR, GO-CFAR and SO-CFAR detectors for $\alpha = 4.7241$, $M = 32$ and $\alpha 0 = 10 - 4$..... 48
Figure 3.5 - Probability of Detection of Optimal, ML-CFAR, GO-CFAR and SO-CFAR detectors for $\alpha = 4.7241$, $M = 16$ and $\alpha 0 = 10 - 4$..... 49
Figure 3.6 – Probability of Detection of Optimal, ML-CFAR, GO-CFAR and SO-CFAR detectors in presence of a single interfering target with $ICR = 20$dB for $\alpha = 4.7241$, $\alpha 0 = 10 - 4$ and $M = 16$..... 51
Figure 3.7 – Probability of Detection of Optimal, ML-CFAR, GO-CFAR and SO-CFAR detectors in presence of a single interfering target with $ICR = 20$dB for $\alpha = 4.7241$, $\alpha 0 = 10 - 4$ and $M = 32$..... 51
Figure 3.8 – Probability of Detection of Optimal, ML-CFAR, GO-CFAR and SO-CFAR detectors in presence of a single interfering target with $ICR = 40$dB for $\alpha = 4.7241$, $\alpha 0 = 10 - 4$ and $M = 32$..... 52
Figure 3.9 – Probability of Detection of Optimal, ML-CFAR, GO-CFAR and SO-CFAR detectors in presence of two interfering targets both located in one-half reference window with $ICR1 = 20$dB, $ICR2 = 40$dB, $\alpha = 4.7241$, $\alpha 0 = 10 - 4$ and $M = 32$. 53
Figure 3.10 – Probability of Detection of Optimal, ML-CFAR, GO-CFAR and SO-CFAR detectors with one interfering target in each half of the reference window with $ICR1 = 20$dB, $ICR2 = 40$dB, $\alpha = 4.7241$, $\alpha 0 = 10 - 4$ and $M = 32$..... 54

Introduction

A. Preamble

The main function of a radar communication system is to detect targets within a certain distance using emitted and reflected high-frequency radio waves (or electromagnetic EM waves). In fact, the word "radar" is an acronym for "***ra****dio* ***d****etection* ***a****nd* ***r****anging*". Indeed, technological advances in electronics and computer science have greatly contributed to the advancement of radars. As a result, radar detection has become one of the main applications of radar signal processing and has attracted much attention for many years.

In fact, the detection target signals in random noise is a very challenging task. This task becomes increasingly difficult in presence of unwanted echoes, such as clutter, jamming and interferences. The presence of such reverberations makes the separation of target signal difficult from these interfering noises. It has been shown that such problems can be formulated mathematically as binary decision problems. The latter is a branch of probability theory.

B. Historical Background

The history of radar began more than one hundred and fifty years ago, with the researches of the British physicist James Clerk Maxwell, in 1864. Maxwell showed theoretically that radio waves possess some properties resembling those of light waves. This was proved experimentally later in 1886 by the German physicist Heinrich Rudolf Hertz. As predicted theoretically by Maxwell, Hertz discovered and showed that the EM waves traveled at the speed of light and could be reflected, refracted, diffracted from various objects, and can be polarized like visible light waves.

The amazing discovery inspired researchers across the world. In 1901, the Italian inventor Guglielmo Marconi successfully sent radio signals across the Atlantic. This was

the birth of modern communications industry. In 1904, the German engineer Christian Hulsmeyer first proposed the use of radio echo in a detection device to avoid collisions in navigation [1, 2]. Then, in 1917, Nikola Tesla developed the theoretical foundations for the future radar. Later, during the Second World War, Sir Robert Watson-Watt was able to build a radio detector that the Americans named "RADAR", which stands for "RAdio Detection And Ranging". During the following years, various experimenters in EM waves has been carried out, which contributes to the gradual development of radar [1, 2].

C. Motivations

As mentioned before, radar target detection is a topic of great importance in various civil and military fields. Nowadays, the demand of more sophisticated detection algorithms has been increased significantly especially with the huge progress made in radar system electronics. It is well known that radar systems are operating in open environment and will receive returns echoes from many sources. In addition to reflections from targets (objects of interest), the radar signal includes unwanted echoes, known as *clutter,* backscattered from the environment and other unwanted objects. Thus, the radar system inevitably processes target signal in the presence of undesired clutter.

Indeed, clutter is a random process, which is the main source of detection errors. Thus, separating the target signal from the clutter is a key task, which will help significantly to mitigate the effect of these errors. To do so, a good mathematical and physical description of clutter is essential. Due to random nature of clutter, the theory of probability, which is a branch of mathematics, represents the natural framework for radar detection problem. It has been also shown that statistical modeling by means of probability distributions can provides a physical context for relating the characteristics of

clutter to its random behavior. Thus, statistical clutter modeling is essential and basic for calculating and optimizing the performance of radar detectors.

D. State of the Art

The literature currently offers several studies regarding CFAR detection in Pareto-distributed clutter. In addition to its appropriate statistical description of sea clutter echoes, the analytical simplicity of the Pareto model makes it more practical [3, 4], particularly for developing full CFAR detection algorithms, compared to other non-Gaussian models such as Log-normal, Weibull, Gamma and *K* models [5, 6, 7, 8].

It is therefore of great interest to study the CFAR detection problem under the assumption of a Pareto distribution clutter. In fact, Weinberg [9] has proposed a new methodology that exploits the natural relationship between the two distributions, Exponential and Pareto, to develop non-conventional processors for non-coherent CFAR detection in the case of a distributed Pareto clutter.

Based on this duality between both laws, these CFAR detectors are fundamentally related to some conventional detectors for the Gaussian case [10, 11]. In [9, 12, 13, 14, 15], some CFAR detection approaches were proposed for a Pareto distributed clutter, assuming a priori knowledge of the scaling factor parameterizing this distribution. The optimal detector was also discussed in [16, 17].

The first non-conventional CFAR detector proposed by Weinberg is the GM-CFAR (Geometric Mean-CFAR) detector [9]. In this type of detector, the clutter level is estimated using the product (or the geometric mean) of the cells in the reference window. The major disadvantage of the GM-CFAR detector is that, when the environment is heterogeneous, the detection threshold increases and the probability of detection (P_d) decreases even for high values of the Signal-to-Clutter ratio, SCR.

For all these detectors, the relationships between false alarm probability and adaptive threshold are completely preserved when transforming decision rules from Gaussian to Pareto case. However, there is a crucial difference in the formulation and definition of the adaptive threshold between both cases: Gaussian and Pareto.

Unfortunately, all these strategies don't really act as true CFAR procedures, since they were mainly based on the assumption of a scale parameter known a priori. This limits their use in realistic cases where the clutter parameters are unknown a priori. Moreover, this explicit dependence on the scale parameter of the Pareto law is a direct result of the transformation used to develop CFAR detectors for a distributed Pareto clutter. Although the scale parameter is of little importance in determining the shape of the distribution, it seems important in practice and for more realistic cases to develop CFAR detectors that are entirely independent of all clutter parameters. For this reason, we propose to modify the optimal detector by using the Maximum likelihood estimates of clutter parameters. This leads to a modified detector, which will be called Maximum Likelihood (ML) CFAR detector. Note that the optimal detector is based on the prior knowledge of these parameters, which makes it unpractical for real situations. In fact, this detector has been originally proposed by Sahed [18], and was the subject of Weinberg's work in [13].

E. Organization of the Dissertation

This dissertation analyses the performance of some radar CFAR detection approaches operating over a Pareto-Distributed clutter, beginning with the theoretical concept and concluding with a simulated implementation.

In Chapter 1, a general description of the process begins by providing some basics of radar detection in noise. Chapter 2 describes analytically some Mean-Level CFAR detectors and gives the mathematical derivations of their probability of false alarm. In

Chapter 3, we validate, test and examine the performance of such detectors via numerical simulations. The obtained results are discussed and interpreted in the same chapter, as well. At the end of the dissertation, we give some conclusions and recommends future works.

Chapiter 1 : Basics of Radar Signal Detection in Noise

1.1 Introduction

Throughout this chapter, we provide a general overview about signal detection in noise and its relation to binary decision theory. After that, we discuss the problem of statistical modeling of different radar signals (i.e, target signals and Noise/clutter echoes). In fact, statistical modeling is important, because it is necessary in the establishment of decision rules. At the end of this chapter, we present the principle of CFAR decision rules, which widely used in radar communications systems and in many remote sensing devices.

1.2 Binary Detection theory

Target detection is fundamental in radar systems. In a typical radar receiver, the returned echo is received by the antenna and then passed through an envelope-detector. The detector separates the envelope of the signal, which contains both the desired signal and the unwanted echoes such as receiver noise, clutter and interferences.

In general, the detection of a radar signal in noise can be formulated as a binary hypothesis test. In such case, the received signal can be given as

$$\begin{cases} Y = N & for\ H_0(missing\ target) \\ Y = S + N & for\ H_1(present\ target) \end{cases} \tag{1.1}$$

where Y, S and N are complex random variables representing respectively the complex envelope (or the amplitude) of the received signal, the useful signal of the target and the noise, H_0 denotes the null hypothesis, which is the hypothesis that the received signal is due to noise only, while H_1 denotes the alternative hypothesis, which is the hypothesis that the received signal is due to a target return plus noise [17, 19].

In order to obtain a decision regarding the presence or absence of a target, the null hypothesis, H_0, should be tested against the alternative one H_1. This kind of tests can lead to establish two key metrics, which will be used later in performance evaluation and assessment of different decision rules. The first one is the probability of false alarm, P_{fa}, which is to decide H_1 while hypothesis H_0 is true, and the probability of detection, P_d, which is to decide H_1 while hypothesis H_1 is true [17, 19].

1.3 Radar Signal Modeling

1.3.1 Clutter modeling

As mentioned previously, clutter modeling is essential in the design of radar target detectors. This is because the radar operates inside a given environment and sometimes it is surrounded by unwanted objects. Reflections from environment (i.e, clutter) and from undesired objects (interferences), as well, are the main sources of errors during the process of detection. Thus, knowing the mathematical nature and physical behavior of these unwanted signals is very important in order to mitigate their effects. Statistical modeling is a key tool that can provide a good mathematical description and an acceptable physical interpretation of physical phenomena related to clutter random behavior. The objective of clutter modeling is simply finding the probability laws (or probability density functions, pdf) that describe the actual distribution of clutter amplitudes or intensities.

1.3.1.1 Gaussian models of clutter

At the beginning of radar systems, Gaussian models of sea clutter were the only ones, from which they achieved convincing success relative to the known applications at that time. This classical statistical description of the sea surface is based on a

representation of wave slopes and heights in terms of stationary Gaussian random fields [17].

a. Normal Distribution

The normal or Gaussian distribution, shown in Figure 1.1, is defined by [20]

$$f_X(x) = \frac{1}{\sigma\sqrt{2\pi}} \exp\left(-\frac{1}{2}\left(\frac{x-\mu}{\sigma}\right)^2\right), \quad x \geq 0 \tag{1.2}$$

where μ is the mean and σ² is the variance.

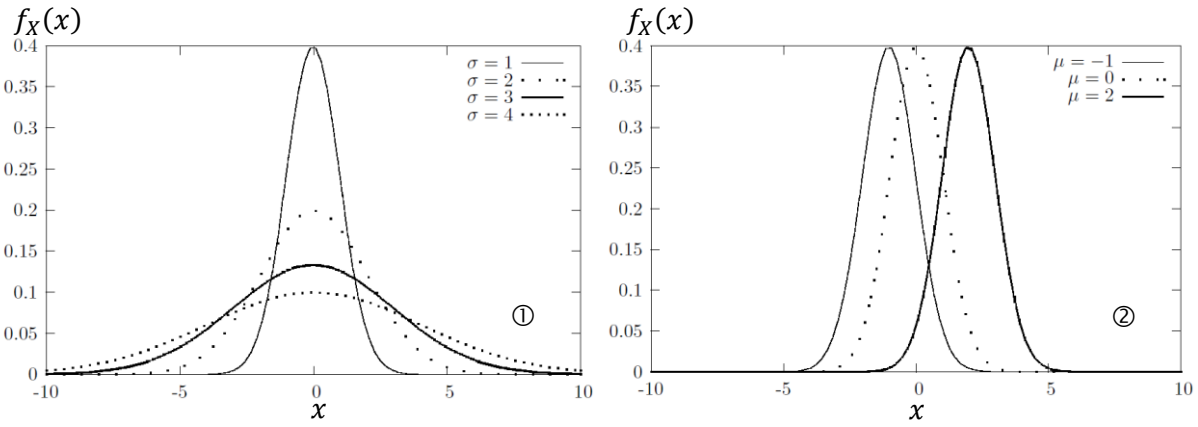

Figure 1.1 - Probability density function of the Gaussian law (①μ=0 ②σ=1)

a. Rayleigh distribution

The Rayleigh distribution is a part of the Gaussian laws and is defined by [20]

$$f_X(x) = \frac{x}{b} \exp\left(\frac{-x^2}{b}\right), \quad x > 0 \tag{1.3}$$

where b is a scale factor.

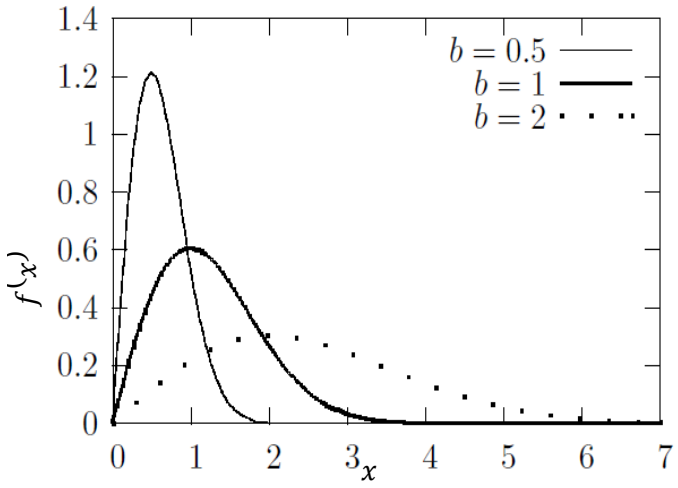

Figure 1.2 - Probability density function of Rayleigh distribution

1.3.1.2 Non-Gaussian Clutter Models

a. Log-Normal Distribution

The Log-Normal distribution is provided by [20]

$$f_X(x) = \frac{1}{\sqrt{2\pi\sigma x}} \exp\left(-\frac{(\ln(x)-\mu)^2}{2\sigma^2}\right), \quad x \geq 0 \tag{1.4}$$

where μ is the mean of $ln(x)$ and σ^2 is the variance

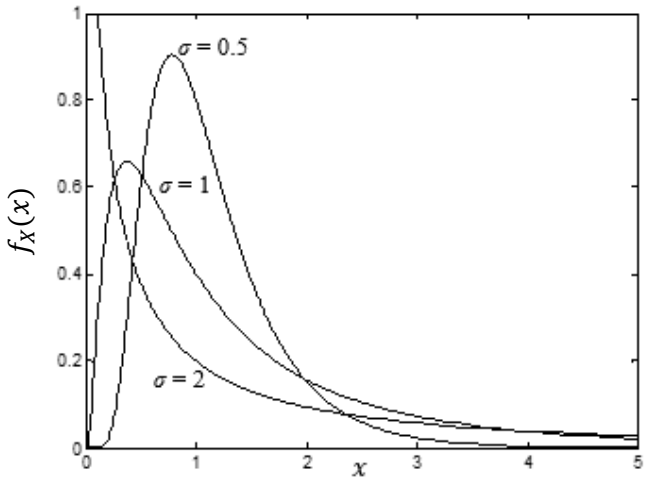

Figure 1.3 - Probability density function of the Lognormal distribution

b. Weibull distribution

Weibull distribution is given by [20]

$$f_x(x) = \frac{c}{b}\left(\frac{x}{b}\right)^{c-1} exp\left[-\left(\frac{x}{b}\right)^{c}\right] \tag{1.5}$$

where b is the scale parameter and c is the shape parameter.

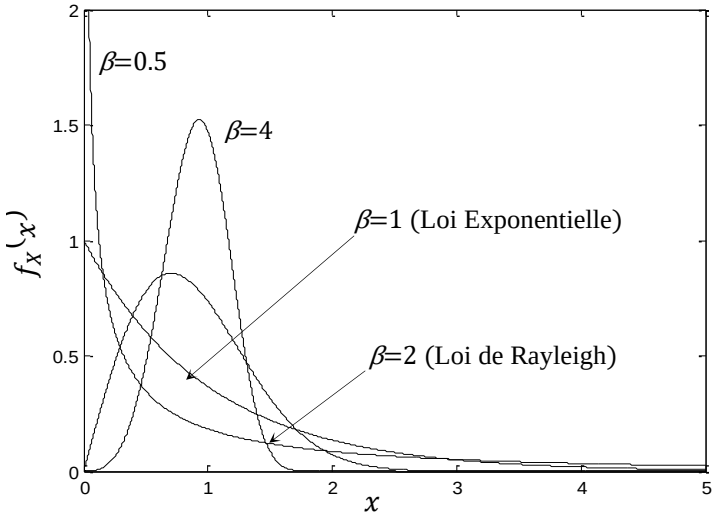

Figure 1.4 - Probability density function of the Weibull distribution

c. K-distribution

This K-distribution is defined as follows [20]

$$f_x(x) = \frac{4}{b\Gamma(c)}\left(\frac{x}{b}\right)^{c} K_{c-1}\left(\frac{2x}{b}\right), \quad x \geq 0 \tag{1.6}$$

Where b is a scale parameter, c is a shape parameter, $\Gamma(\cdot)$ is the gamma function, and $K_c(\cdot)$ is the modified Bessel function.

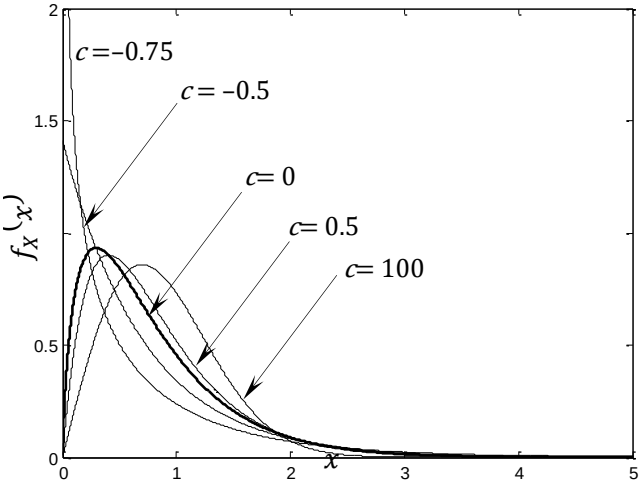

Figure 1.5 - Probability density function of the *K* distribution

d. Simple Pareto distribution

The simple Pareto distribution has recently been validated as a statistical model for high-resolution sea clutter return echoes. The probability density function (pdf) given by [20]:

$$f_X(x) = \begin{cases} \dfrac{\alpha\beta^{\alpha}}{x^{\alpha+1}} & si \quad x \geq \beta \\ 0 & si \quad x < \beta \end{cases} \tag{1.7}$$

where α is a shape parameter and β is a scale factor.

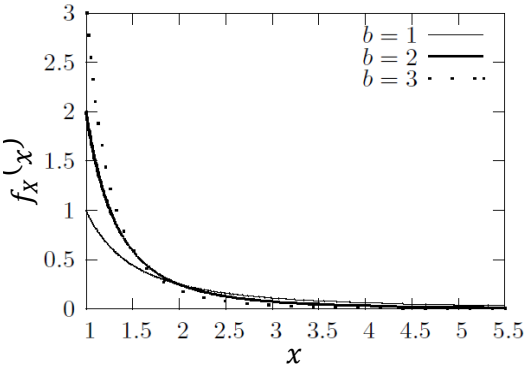

Figure 1.6 - Probability density function of the Pareto distribution.

1.3.2 Target Modeling

The amplitude of the target signal at the receiver depends on the target radar cross section (RCS), which is the effective scattering area of a target as seen by the radar. In general, the target RCS fluctuates because targets consist of many scattering elements, and returns from each scattering element vary [21]. The effect of the fluctuation is to require a higher signal-to-noise ratio for high probability of detection, and lower values for low probability of detection than those required with no fluctuating signals. In addition, returns from the same scattering element are functions of the illumination angle, the frequency and polarization of the transmitted wave, the target motion and vibration, and the kinematics associated with the radar itself.

Target RCS fluctuations are often modeled according to the four Swerling target cases, Swerling case 1 to 4. These fluctuating models assume that the target RCS fluctuation follows either a Rayleigh or one-dominant-plus Rayleigh distribution with scan-to-scan or pulse-to pulse statistical independence [21].

1.3.2.1 Swerling I Model

In this case, the returned signal power per pulse on any one scan is assumed to be constant, but these echo pulses are independent (uncorrelated) from scan to scan. A returned signal of this type is then a scan-to-scan fluctuation.

The envelope of the entire pulse-train is a single Rayleigh-distributed independent random variable given by [21]

$$p_{\sigma}(\sigma) = \frac{1}{2\bar{\sigma}^2} exp\left(\frac{-\sigma}{2\bar{\sigma}^2}\right), \quad \sigma \geq 0 \tag{1.8}$$

where σ is the average Radar Cross Section (RCS) (average of RCS or signal-to-noise power ratio σ) over all target fluctuations.

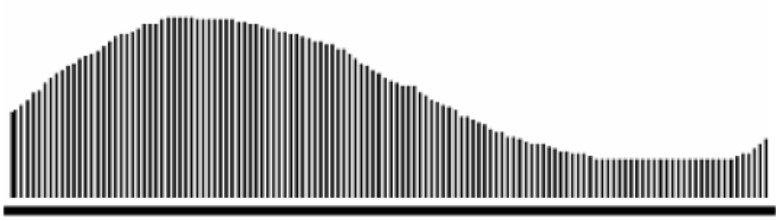

Figure 1.7 - Swerling Model I

1.3.2.2 Swerling II Model

In this case, the fluctuations are more rapid than in the Swerling I model, and are assumed to be independent from pulse-to-pulse instead of from scan-to-scan. This is pulse-to-pulse fluctuation. The probability density function for the target cross section is the same as given in (1.8) [21].

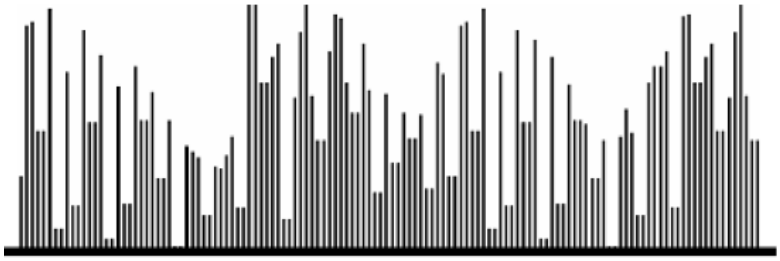

Figure 1.8 - Swerling Model II

1.3.2.3 Swerling III model

As in the case of a Swerling I model, the fluctuations are independent from scan to scan, but the pdf is given now by [21]

$$p_\sigma(\sigma) = \frac{4\sigma}{\bar{\sigma}^2} exp\left(\frac{-2\sigma}{\bar{\sigma}^2}\right), \ \ \sigma \geq 0 \tag{1.9}$$

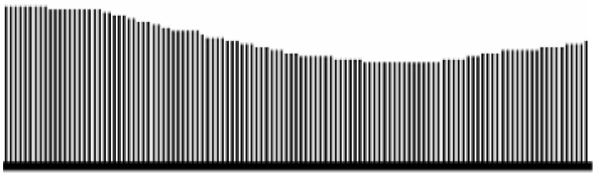

Figure 1.9 - Swerling Model III

1.3.2.4 Swerling IV Model

In this case, the fluctuations are pulse-to-pulse as in Swerling II case, but the probability density function is given by (1.9) [21].

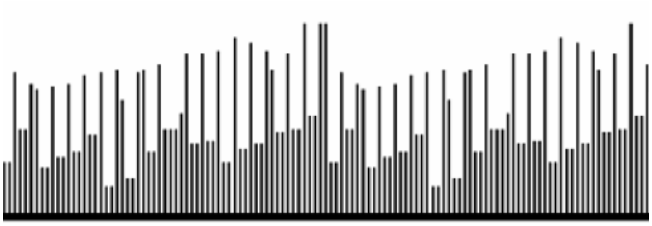

Figure 1.10 - Swerling Model IV

1.4 Optimal Neyman-Pearson detector

A decision rule can be now designed based on the Neyman-Pearson criterion [19]. The optimum Neyman-Pearson detector is depicted in Figure 1.1. Where $r(t)$ denotes the received signal and ω_c the carrier angular frequency. The input signal at the receiver, when a target is present, is an attenuated, randomly phase shifted version of the transmitted pulse embedded in white Gaussian noise. The received signal $r(t)$ is processed by the inphase and quadrature channels

The Neyman-Pearson criterion requires that the probability of false alarm, P_f, is less than a desired value, α_0, and that the probability of target detection should be maximized. This results in the likelihood ratio test, that is [19]

$$\Lambda(q) = \frac{f_Q\,(q|H_1)}{f_Q(q|H_0)} \underset{H_0}{\overset{H_1}{\gtrless}} \lambda \tag{1.10}$$

where $\Lambda(q)$ is the likelihood ratio, $f_Q\,(q|H_i)$ is the conditional pdf, of Q when hypothesis $H_0,\ i = 0,1$ is true, and λ is the detection threshold which is obtained from the constraint $P_{fa} = \alpha_0$, that is [19]

$$\int_{\lambda}^{+\infty} P_{\Lambda}(l|H_0)d\lambda = \alpha_0 \tag{1.11}$$

+

The solution of (1.11) yields a threshold which is a function of the noise variance.

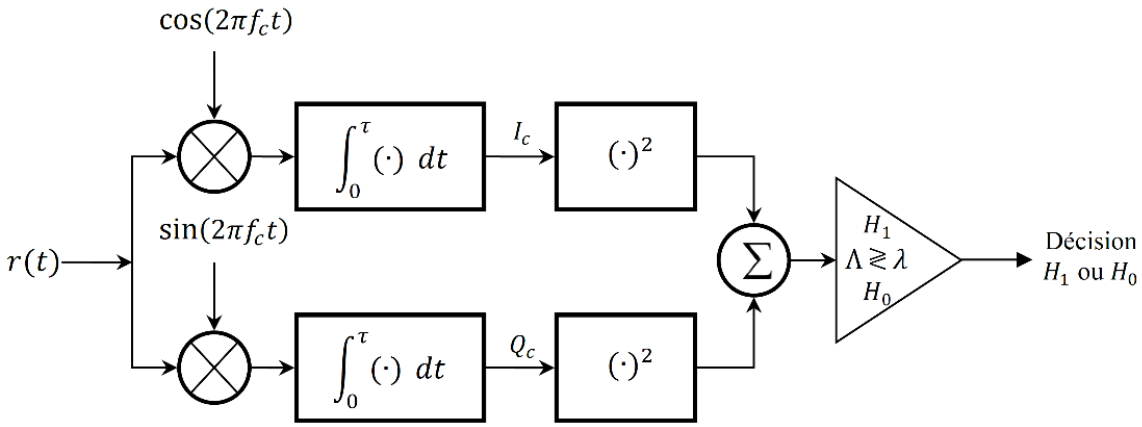

Figure 1.11 - Optimum Neyman-Pearson detector

1.5 CFAR Detection

The constant false alarm rate (CFAR) technique aims to adaptively adjust the detection threshold to control the false alarm rate in the presence of uncertainty in clutter power level.

1.5.1 Formulation of the CFAR detection problem

In the absence of clutter or in a uniform clutter, this task is easily fulfilled by setting an overall detection threshold. However, in a non-uniform clutter, the false alarm rate can vary significantly if a fixed threshold detector is used. To maintain constant performance in a non-stationary medium, the radar must locally estimate the power of the

clutter to set a local threshold, called adaptive. This is the principle of adaptive detectors with constant false alarm rate CFAR (Constant False Alarm Rate) [10, 22].

1.5.2 Principle of CFAR detectors

In a CFAR detector, the received signal is sampled in distance and sent to a shift register to form the reference window. This window is a sliding window composed of M neighboring cells surrounding a cell under test, CUT, with M being an even number.

The CUT divides the reference window into two half-windows, the lagging half-windows and the leading half-windows, each of length $N = M/2$. The clutter power in the CUT is estimated based on the observations in the reference window. The detection threshold is determined by multiplying the estimated clutter power Z by a multiplication factor T. This ensures that the desired false alarm probability is maintained. The CFAR detector uses a detection test or hypothesis test to identify the resolution cells that are likely to be targets. The performance of this hypothesis test can be characterized in terms of P_{fa} and P_d [19, 21, 10, 23].

1.5.3 Decision rule in a CFAR detector

In the case of homogeneous clutter, the M samples $x_1, x_2, \ldots\ldots, x_M$ in the M neighboring cells of the reference window of the CFAR detector are statistically independent and identically distributed (iid), and are independent of the CUT statistic z_0. A statistical test, denoted Z, is formed from the samples $x_1, x_2, \ldots\ldots, x_M$, which represents an estimate of the average power level of the clutter in the CUT. This estimate is multiplied by a thresholding constant T, which is chosen so as to guarantee a certain desired false alarm probability $P_{fa}(T) = \alpha_0$. This results in an adaptive detection threshold. To make a decision on the presence or absence of a target in the CUT [19], the

content of the latter, denoted Z_0, is compared to the threshold adaptive according to a binary decision rule.

$$\begin{matrix} H_1 \\ Z_0 \gtrless TZ \\ H_0 \end{matrix} \tag{1.12}$$

The CFAR detector uses a binary decision rule to compare the content of the CUT, denoted Z_0, with an adaptive detection threshold, which is totally independent of the clutter parameters to ensure a constant false alarm rate. The detection threshold is calculated based on the pdfs of the two statistic $Z_0|H_0$ and Z [19, 23, 16].

To evaluate the performance of a CFAR detector, the false alarm probability, P_{fa}, and the detection probability, P_d, are often used. The pdfs of the statistical test Z, and the content of the CUT, Z_0, under the two hypotheses H_0 and H_1 respectively, are used to calculate P_{fa} and P_d [18, 17, 16].

$$P_{fa} = \Pr(Z_0 > TZ|H_0) = \int_0^\infty \left[\int_{Tz}^\infty p_{Z_0|H_0}(z_0|H_0) dz_0 \right] p_Z(z) dz \tag{1.13}$$

and

$$P_d = \Pr(Z_0 > TZ|H_1) = \int_0^\infty \left[\int_{Tz}^\infty p_{Z_0|H_1}(z_0|H_1) dz_0 \right] p_Z(z) dz \tag{1.14}$$

It is difficult to determine the pdfs of the statistics Z, $Z_0|H_0$ and $Z_0|H_1$, which makes it challenging to calculate the false alarm probability and detection probability. In practice, the user specifies the desired false alarm probability, P_{fa}, denoted as α_0, and the detection threshold value is deduced accordingly.

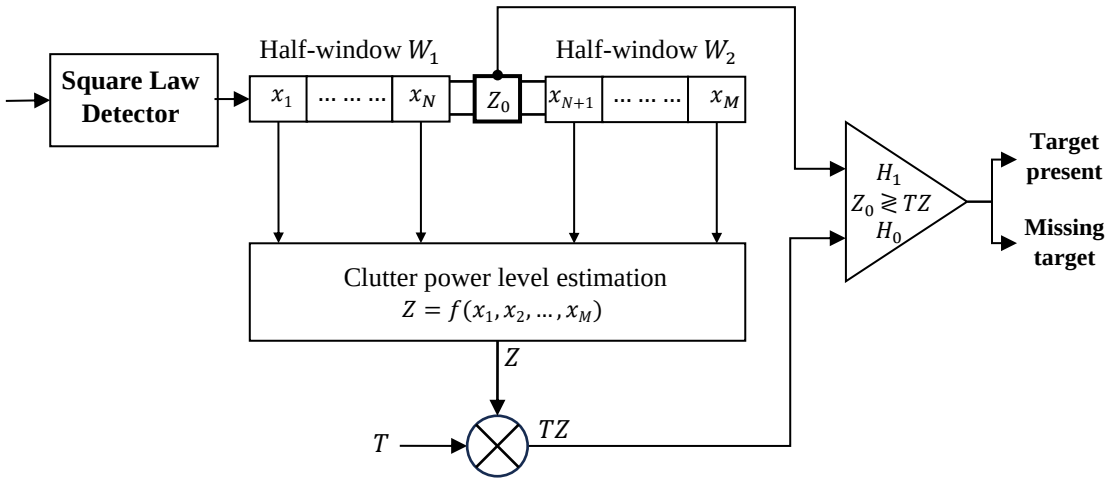

Figure 1.12 - Block diagram of a CFAR adaptive detector

1.6 Conclusion

In this chapter, we have introduced radar clutter models and target models, which are essential for CFAR detection. We discussed some specific models, such as Pareto and other distributions, and explained decision theory. In addition, we give the principle of CFAR detection.

Chapiter 2 : CFAR Detection in Homogenous Pareto-Distributed Clutter

2.1 Introduction

In this chapter, we analyze and assess the performance of some CFAR processors operating over a homogenous Pareto distributed clutter, namely, the Geometric Mean (GM) CFAR, the Greatest-Of (GO) CFAR and the Smallest-Of (SO) CFAR.

In all cases, we assume that all the parameters of clutter are unknown *a priori*. As it will be shown later, the expressions of the false alarm probability are provided, while we proceed to simulation in order to assess the detection probability computing.

2.2 Statistics of the CUT

Herein, we discuss some aspect related to the distribution that characterize the different signals in the CUT under both hypothesis H_0 and H_1. It may be pointed out that the radar system is equipped by a square-law detector before the CFAR window. This assumption is made because the Pareto distribution is an intensity model, which has been validated in the literature to describe the power of the received sea clutter.

Practically, the content of the CUT Z_0 consists either of clutter echo X only or a combination of clutter echo X and target signal return Y. As stated earlier in previous chapter, the detection problem can be formulated as a binary hypothesis testing problem, which may be defined as follows

$$H_0(Clutter\ only): Z_0 = X \tag{2.1}$$

$$H_1(Target + Clutter): Z_0 = Y + X \tag{2.2}$$

where H_0 is the null hypothesis, which indicates that there is no target in the CUT, and H_1 stands for the alternative hypothesis, which states that there is a target and clutter in the CUT.

2.2.1 CUT's Statistics under H_0

In this first case, we suppose that the content of the CUT under H_0, Z_0, is distributed according to the Pareto-distribution. We often denote $Z_0 \triangleq Pa(\alpha, \beta)$ to say that Z_0 is following the Pareto law with shape parameter α and scale parameter β. Hence, the pdf and cdf of Z_0 in this case are given, respectively, by [9, 13]

$$f_{Z_0}(z_0|H_0) = \begin{cases} \dfrac{\alpha\beta^\alpha}{z_0^{\alpha+1}} & si \quad z_0 \geq \beta \\ 0 & si \quad z_0 < \beta \end{cases} \tag{2.3}$$

And

$$F_{Z_0}(z_0|H_0) = 1 - \left(\frac{\beta}{z_0}\right)^\alpha \tag{2.4}$$

2.2.2 CUT's Statistics under H_1

Now, the content of the CUT under hypothesis H_1 defined by (3.2), is due to the contribution of both target returns Y and clutter echoes X. In this dissertation, we assume this a Swerling type I or II fluctuating target whose pdf and cdf are given, respectively, by

$$f_Y(y; \sigma_Y) = \frac{1}{2\sigma_Y^2} \exp\left(-\frac{y}{2\sigma_Y^2}\right) \tag{2.5}$$

And

$$F_Y(y;\sigma_Y) = 1 - \exp\left(-\frac{y}{2\sigma_Y^2}\right) \tag{2.6}$$

where $2\sigma_Y^2$ the average of the target signal power.

By knowing the appropriate models of target signal returns given by (3.6) and clutter echoes, we can now look for the distribution of Z_0 under H_1. Since the signal in the CUT is a combination of target and GM distributed clutter, it is difficult to calculate analytically the pdf of the CUT's content under H_1. For a square-law detector, the complex envelope of the target signal $\boldsymbol{S}$ is added to the complex envelope of clutter echo $\boldsymbol{C}$, and the resulted complex signal is then squared. Accordingly, the CUT output Z_0 can be modelled as the square of the resulted complex signal modulus, which can be given as [24]

$$\begin{aligned} Z_0 \triangleq |\boldsymbol{S}+\boldsymbol{C}|^2 &= |\boldsymbol{S}|^2 + |\boldsymbol{C}|^2 + 2|\boldsymbol{S}||\boldsymbol{C}|\cos(\varphi) \\ &= Y + X + 2\sqrt{Y}\sqrt{X}\cos(\varphi) \end{aligned} \tag{2.7}$$

where $|\cdot|$ is the complex modulus, $Y = |\boldsymbol{S}|^2$, $X = |\boldsymbol{C}|^2$ and φ is a random variable (rv) uniformly distributed on the interval $[0,\ 2\pi]$, which represents here the phase between $\boldsymbol{S}$ and $\boldsymbol{C}$.

Unfortunately, a closed-form expression for the pdf of Z_0 under hypothesis H_1 cannot be derived, which complicates significantly the analysis. Thus, for convenience, we assume that the pdf of clutter in the CUT will be approximated by an exponential distribution with exact same mean power as that of the Pareto-distributed clutter. Accordingly, the content of the CUT, under H_1, is reduced to the sum of an exponential fluctuating target and an exponential distributed clutter. This approximation has

demonstrated high accuracy, which makes it commonly used in the literature [7, 25]. In such case, the resulting signal in the CUT will be also exponentially distributed, and its corresponding conditional pdf can be expressed as

$$f_{Z_0}(z_0|H_1) = \frac{1}{2\sigma_X^2 + 2\sigma_Y^2} \exp\left(-\frac{z_0}{2\sigma_X^2 + 2\sigma_Y^2}\right) \tag{2.8}$$

where $2\sigma_X^2 = \beta/(\alpha - 1)$ is the mean power of Pareto-distributed clutter in the reference cells, and $2\sigma_Y^2$ is the mean power of the exponentially fluctuating target. Now, the signal-to-clutter ratio (SCR) can be defined as

$$\text{SCR} \triangleq \frac{2\sigma_Y^2}{2\sigma_X^2} = \frac{2\sigma_Y^2}{\beta/(\alpha - 1)} \tag{2.9}$$

Hence, the pdf and cdf of $Z_0|H_1$ can be given in terms of SCR, respectively, by

$$f_{Z_0}(z_0|H_1) = \frac{(\alpha - 1)}{\beta(1 + \text{SCR})} \exp\left(-\frac{(\alpha - 1)z_0}{\beta(1 + \text{SCR})}\right) \tag{2.10}$$

and

$$F_{Z_0}(z_0|H_1) = 1 - \exp\left(-\frac{(\alpha - 1)z_0}{\beta(1 + \text{SCR})}\right) \tag{2.11}$$

2.3 Optimal fixed threshold detector

An optimal detector in the Neyman-Pearson sense utilizes a fixed detection threshold, λ, to test the presence or the absence of a target. In doing that, the signal power

level Z_0 in the CUT is compared to λ, according to the following well-known decision rule [18]

$$Z_0 \underset{H_0}{\overset{H_1}{\gtrless}} \lambda \tag{2.12}$$

Based upon (2.12), the performance of the optimal detector can be easily analyzed in the case of a Pareto-distributed clutter.

2.3.1 P_{fa} of the optimal fixed threshold detector

Under H_0, the content of the CUT is $Pa(\alpha, \beta)$, the probability of false alarm of the optimal detector (P_{fa}^{Op}) can be determined as follows

$$\begin{aligned} P_{fa}^{Op} &= \Pr(Z_0 > \lambda | H_0) \\ &= \int_{\lambda}^{\infty} f_{Z_0}(z_0|H_0) dz_0 \\ &= 1 - F_{Z_0}(\lambda|H_0) \\ &= \left(\frac{\beta}{\lambda}\right)^{\alpha} \end{aligned} \tag{2.13}$$

By inverting (2.13), the fixed threshold λ of the optimal detector can be given, for a desired P_{fa}^{Op} equal to α_0, by

$$\lambda = \beta {\alpha_0}^{-\frac{1}{\alpha}} \tag{2.14}$$

It may be noted according to (2.14) that the clutter parameters (α and β) must be known before computing the threshold λ.Thus, the optimal detector is not suitable for practical scenarios. As a result, this detector will be used as a benchmark only to assess the performance of other detectors.

2.3.2 P_d of the optimal fixed threshold detector

In the presence of a target in the CUT, $Z_0|H_0$ follows the exponential distribution defined by (2.10). Therefore, the probability of detection of the optimal detector (P_d^{Op}) can be determined by

$$\begin{aligned} P_d^{Op} &= \Pr(Z_0 > \lambda|H_1) = \int_{\lambda}^{\infty} f_{Z_0}(z_0|H_1)dz_0 \\ &= 1 - F_{Z_0}(\lambda|H_1) = \exp\left(-\frac{(\alpha-1)\lambda}{\beta(1+\mathrm{SCR})}\right) \end{aligned} \tag{2.15}$$

2.4 Geometric Mean (GM) CFAR detector

The GM-CFAR detector is applied here for a homogeneous Pareto-distributed clutter. It estimates the clutter power level in the CUT by multiplying the $M = 2N$ samples in the reference window. This product is closely related to the geometric mean of the *M* samples in the reference window, so the name Geometric Mean CFAR. In the homogeneous case, the GM-CFAR detector is defined using a set of *M* iid random variables distributed according to the Pareto law. In the case of GM-CFAR, the decision rule used to determine whether the signal is present or not can be formulated as follows [9, 13]

$$Z_0 \underset{H_0}{\overset{H_1}{\gtrless}} \beta^{1-MT} \prod_{i=1}^{M} X_i^T \tag{2.16}$$

It may be noted that for the sake of simplicity, we always assume that *M* is an even number throughout the study of all discussed detectors.

We notice that the GM-CFAR detector defined by (2.16) is independent of the shape parameter α, but it depends explicitly on the scale parameter β. This means that the detector is CFAR only with respect to α. However, it is not CFAR with respect to β. Therefore, the GM-CFAR detector does not really act as a true CFAR detector. However, it is recalled here for the purpose of comparison.

Suppose that the CUT and the *M* neighboring cells of the reference window simply contain Pareto distributed clutter, the P_{fa} is then given by

$$P_{fa} = \Pr\left(Z_0 > \beta^{1-MT} \prod_{i=1}^{M} X_i^T \middle| H_0 \right) \tag{2.17}$$

The quantity $\beta^{1-MT} \prod_{i=1}^{M} x_i^T$ is the unconventional adaptive detection threshold of the GM-CFAR detector, which we note λ_{GM} (i.e, $\lambda_{\mathrm{GM}} = \beta^{1-MT} \prod_{i=1}^{M} x_i^T$).

To calculate the P_{fa}, we exploit the duality between the Standard Exponential distribution and the Pareto distribution [13]. Moreover, it was shown in [9, 13] that if $X \triangleq Pa(\alpha, \beta)$ then

$$X = \beta e^{\alpha^{-1}Y} \tag{2.18}$$

where $Y \triangleq Exp(1)$ (i.e, Y is an v.a distributed according to the standard exponential law).

By applying (2.18) it can be shown that $Z_0 = \beta e^{\alpha^{-1}Y_0}$ and $x_i = \beta e^{\alpha^{-1}y_i}$, where $Y_0 \sim Exp(1)$ and $X_0 \sim Exp(1)$, as well. Thus, one can exploit this result to compute the expression of P_{fa}. This can be done simply by introducing the natural logarithmic function to (2.17) as follows:

$$P_{fa} = \Pr\left(\log\left(\frac{Z_0}{\beta}\right) > log\left(\beta^{-MT}\prod_{i=1}^{M} {X_i}^T\right)\middle| H_0\right)$$

$$= \Pr\left(\log\left(\frac{Z_0}{\beta}\right) > T\sum_{i=1}^{M} log\left(\frac{X_i}{\beta}\right)\middle| H_0\right) \tag{2.19}$$

Now it can be seen that the decision rule is changed and takes the form of the well-known CA-CFAR decision rule, which operated over Gaussian noise [10, 19, 22] . So, if we set $Y_0 = \log\left(\frac{Z_0}{\beta}\right)$ along with $Y_i = log\left(\frac{X_i}{\beta}\right)$, the transformed decision rule can be given according to the following form:

$$Y_0 \underset{H_0}{\overset{H_1}{\gtrless}} T\sum_{i=1}^{M} y_i \tag{2.20}$$

Now, the P_{fa} can be computed simply as follows

$$P_{fa} = \Pr\left(Y_0 > T\sum_{i=1}^{M} Y_i \middle| H_0\right)$$

$$= \int_0^{+\infty}\left[\int_{Tq}^{+\infty}(Y_0|H_0)dy_0\right] f_Q(q)dq$$

$$= 1 - \int_0^{+\infty} F_{Y_0}(Tq|H_0)\, f_Q(q)dq \qquad (2.21)$$

$$= 1 - \int_0^{+\infty}[1 - e^{-Tq}]\frac{1}{\Gamma(M)}\, q^{M-1}\exp(-q)\, dq$$

$$= 1 - \int_0^{+\infty} f_Q(q)dq + \int_0^{+\infty}\frac{1}{\Gamma(M)}\, q^{M-1}\exp(-q-Tq)\, dq$$

$$= \frac{1}{\Gamma(M)}\int_0^{+\infty} q^{M-1}\exp(-q(1+T)\, dq$$

$$= \frac{1}{\Gamma(M)}\,\frac{1}{(1+T)^M}\Gamma(M)$$

At the end, we obtain

$$P_{fa} = (1+T)^{-M} \qquad (2.22)$$

Moreover, for a desired P_{fa} equal to α_0, the scalar factor T of the GM-CFAR detector is given, after inversion of (2.22), by

$$T = \alpha_0^{-\frac{1}{M}} - 1 \tag{2.23}$$

On the other hand, the P_d can be computed using Monte-Carlo simulation by assuming that the useful signal of the target is added coherently to the Pareto-distributed clutter in the CUT, according to

$$P_d = \Pr\left(Z_0 > \beta^{1-MT} \prod_{i=1}^{M} x_i^T \middle| H_1 \right) \tag{2.24}$$

However, in this case, the P_D should be evaluated based on the Monte-Carlo simulation method. Choice which is, unfortunately, unique in the absence of an analytical expression of the pdf of the statistic $Z_0|H_1$ [18].

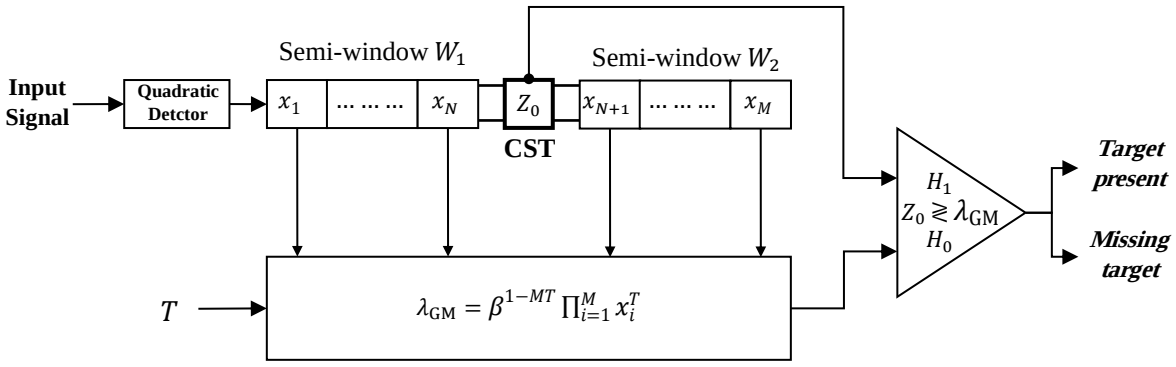

Figure 2.1 - Block diagram of the GM-CFAR detector

2.5 Maximum Likelihood (ML) CFAR detector

In this subsection, we discuss and analyze the ML-CFAR detector with unknown shape parameter. This detector is initially proposed by Sahed [18] and is the subject of work published by Weinberg in [13]. It is simply a modified version of the GM-CFAR detector with known shape parameter discussed previously. The main difference between GM-CFAR and ML-CFAR is that the former is more practical, since it doesn't depend on any of the clutter parameters.

Herein, the estimation of the power level of clutter in the CUT is carried out using the geometric mean of the M samples in the reference window and their minimum. Unlike the GM-CFAR detector, which does not ensure the CFAR property without absolute knowledge of the scale parameter, the ML-CFAR discussed here proves to be more practical, hence it fulfills this property compared to to all unknown parameters of the distributed Pareto clutter. The block diagram of the ML-CFAR detector is summarized in Figure 2.2.

Consider in the homogeneous case, a set $\{x_i: i = 1, 2, \dots, M\}$ of M iid random variables distributed according to the Pareto law. The ML-CFAR detector is therefore defined by [13, 18]

$$Z_0 \underset{H_0}{\overset{H_1}{\gtrless}} x_{(1)}^{1-MT} \prod_{i}^{M} x_i^T \tag{2.25}$$

where $x_{(1)} \triangleq Pa(\alpha M, \beta)$ is the smallest sample among the M samples of the reference window ($x_{(1)} = \min\{x_1, x_2, \dots, x_M\}$). Note also that it is obvious that the ML-

CFAR detector is a generalization of the GM-CFAR detector, simply replacing β by its maximum likelihood estimator (i.e.,$\hat{\beta}_{ML} = x_{(1)}$).

Like any CFAR detection scheme, we can appreciate the quality of the ML-CFAR detector by its ability to detect a target when the P_{fa} is constant. First, we will determine an expression of the P_{fa} for the ML-CFAR detector assuming that there is only Pareto clutter distributed in the CUT and in the neighboring M cells. So, it is therefore necessary to adjust the detection threshold ensuring a P_{fa} fixed by the user such that [13, 18]

$$P_{fa} = \Pr\left(Z_0 > x_{(1)}^{1-MT} \prod_i^M x_i^T \,\middle|\, H_0\right) \tag{2.26}$$

To calculate the P_{fa}, we always exploit the duality defined by (2.18) between the two Exponential and Pareto distributions. By applying this duality on the three Pareto distributed random variables that appeared in (2.26) (i.e, $Z_0 = \beta e^{\alpha^{-1} Y_0}$, $x_i = \beta e^{\alpha^{-1} y_i}$ and $x_{(1)} = \beta e^{\alpha^{-1} y_{(1)}}$) then by introducing the natural logarithmic function, the P_{fa} can then be calculated as follows

$$\begin{aligned} P_{fa} &= \Pr\left(Y_0 > y_{(1)} + T \sum_{i=1}^M \left(y_i - y_{(1)}\right) \middle| H_0\right) \\ &= \Pr\left(Y_0 > y_{(1)} + TQ \middle| H_0\right) \end{aligned} \tag{2.27}$$

or $f_{Y_0}(y_0) = e^{-y_0}$, $f_{Y_i}(y_i) = e^{-y_i}$, $f_{y_{(1)}}(t) = Me^{-Mt}$ et $Q = \sum_{i=1}^M \left(y_i - y_{(1)}\right)$.

It has already been shown in [13] that the random variable Q is distributed according to the following Gamma distribution:

$$f_Q(q) = \frac{1}{\Gamma(M)} q^{M-1} e^{-q} \tag{2.28}$$

and we note $Q \triangleq \Gamma(M, 1)$

Equation (2.28) can then be rewritten as follows

$$\begin{aligned}
P_{fa} &= Pr\left(Y_0 > y_{(1)} + TQ \middle| H_0\right) \\
&= M \int_0^\infty e^{-Mt} Pr\left(Y_0 > t + TQ \middle| \{y_{(1)} = t\}\right) dt \\
&= M \int_0^\infty e^{-Mt} \int_0^\infty p_Q(q)\, Pr(Y_0 > t + Tq) dt dq \\
&= M \int_0^\infty e^{-Mt} \int_0^\infty p_Q(q) \left[\int_{t+Tq}^\infty e^{-y_0}\, dy_0\right] dt dq \\
&= M \int_0^\infty \mathrm{e}^{-(M+1)t} dt \int_0^\infty p_Q(q)\, e^{-Tq} dq \\
&= \frac{1}{\Gamma(M)} \frac{M}{M+1} \int_0^\infty q^{M-1} e^{-(1+T)q}\, dq
\end{aligned} \tag{2.29}$$

After solving the integral of (2.29), we get

$$P_{fa} = \frac{M}{M+1} (1+T)^{-M} \tag{2.30}$$

By inverting this expression, it is then possible to determine the scalar factor T of the ML-CFAR detector which corresponds to a P_{fa}= α_0 chosen by the user, hence

$$T = \left(\frac{M+1}{M}\alpha_0\right)^{-\frac{1}{M}} - 1 \tag{2.31}$$

However, as for the GM, the P_d of the ML must be evaluated based on the Monte-Carlo simulation method according to

$$P_d = \Pr\left(Z_0 > x_{(1)}^{1-MT}\prod_i^M x_i^T \middle| H_1\right) \tag{2.32}$$

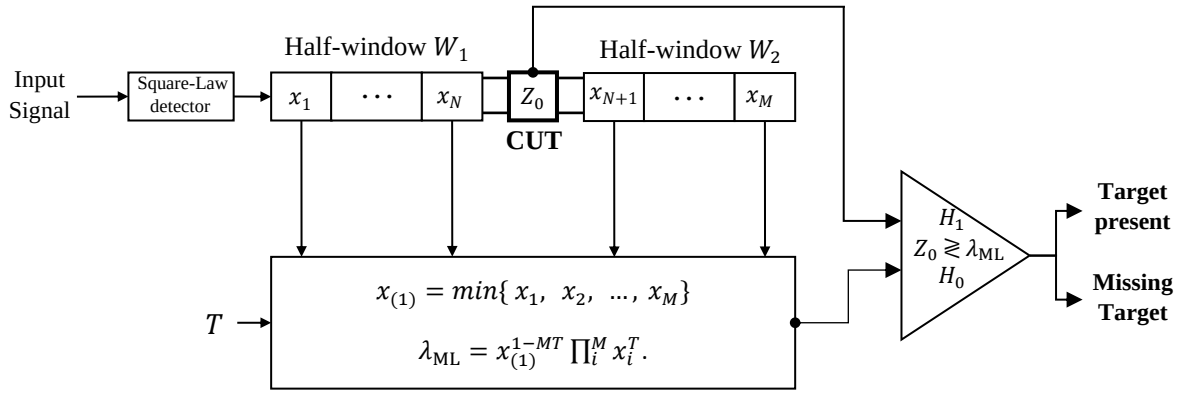

Figure 2.2 - Block diagram of the ML-CFAR detector

2.5 Greatest of (GO) CFAR detector

In a GO-CFAR detector, the local clutter power level is estimated by selecting the maximum of the sample products in the two half-windows, W_1 and W_2, before and after the CUT respectively [12]. This is clearly shown in Figure 2.3. Thus, by transforming the equivalent GO-CFAR detector result from the Gaussian case [12], GO-CFAR takes the following form [12]

$$Z_0 \underset{H_0}{\overset{H_1}{\gtrless}} \beta^{1-NT}[max(W_1, W_2)]^T \tag{2.33}$$

where

$$W_1 = \prod_{i=1}^{N} x_i^T \tag{2.34}$$

and

$$W_2 = \prod_{i=N+1}^{M} x_i^T \tag{2.35}$$

Similar to the GM-CFAR detector, we clearly see the explicit dependence of the statistical test (2.33) on the clutter's scaling parameter β. Consequently, the GO-CFAR detector cannot fulfill the CFAR property, when this parameter is not known a priori.

To evaluate the P_{fa}, it is always assumed that the CUT and the M neighboring cells in the two reference semi-windows are dominated by the distributed Pareto clutter. In this case, according to the decision test (2.33), the P_{fa} is given by

$$P_{fa} = \Pr\left(Z_0 > \beta^{1-NT} \left[max\left(\prod_{i=1}^{N} x_i \, , \prod_{i=N+1}^{M} x_i \right) \right]^T \middle| H_0 \right) \tag{2.36}$$

By applying duality (2.18) on the two Pareto distributed random variables Z_0 and appeared in (2.36) (i.e, $Z_0 = \beta e^{\alpha^{-1}Y_0}$ and $x_i = \beta e^{\alpha^{-1}y_i}$) then introducing the Napierian logarithmic function, the decision rule (2.33) can then be transformed to the following form:

$$Y_0 \underset{H_0}{\overset{H_1}{\gtrless}} T\, max(U,V) \tag{2.37}$$

Or

$$U = \sum_{i=1}^{N} x_i \tag{2.38}$$

and

$$V = \sum_{i=N+1}^{M} x_i \tag{2.39}$$

This rule is exactly the same as that established for the case of a GO-CFAR detector operating in Gaussian noise [10]. We can therefore conclude that the relationship between the P_{fa} and the multiplier T of the Gaussian case is obviously preserved for the Pareto case when applying the logarithmic transformation. Based on (1.13), the P_{fa} of the GO-CFAR detector is given by [12]

$$P_{fa} = 2(1+T)^{-N} - 2\sum_{r=0}^{N-1} \binom{N+r-1}{r} (2+T)^{-(N+r)} \tag{2.40}$$

Since the useful target signal adds coherently to the Pareto distribution clutter in the CUT, the P_d se calculates as follows:

$$P_d = \Pr\left(Z_0 > \beta^{1-NT} \left[max\left(\prod_{i=1}^{N} x_i \, , \prod_{i=N+1}^{M} x_i \right) \right]^T \middle| H_1 \right) \qquad (2.41)$$

However, the P_d cannot be given in a compact analytical form, but must instead be evaluated empirically based on the Monte-Carlo simulation method. This is due to the absence of an analytical expression for the pdf of the statistic $Z_0|H_1$.

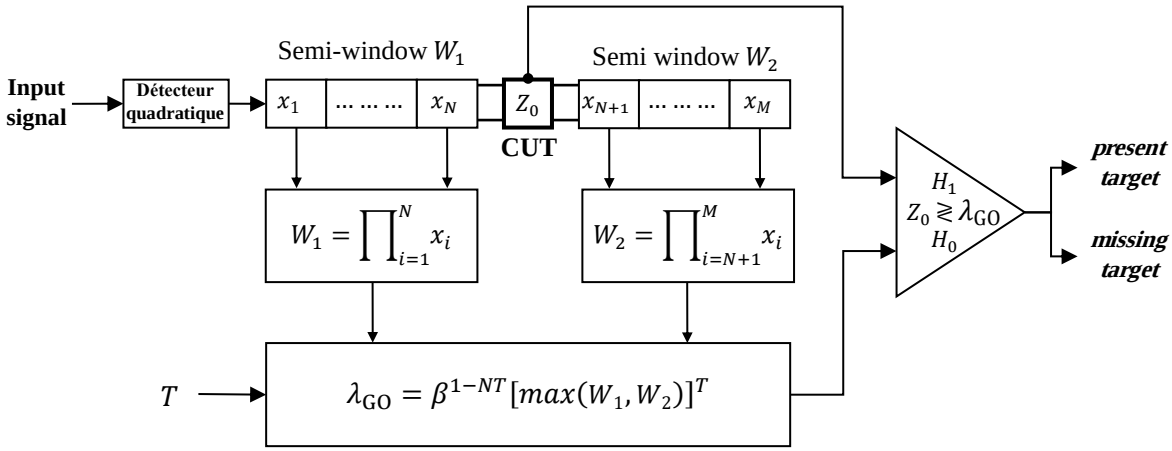

Figure 2.3 - Block diagram of the GO-CFAR detector

2.6 Smallest of (SO) CFAR detector

In this section, we will briefly present the main features of the Smallest-Of (SO) CFAR detector as applied to Pareto environments. Unlike the GO-CFAR detector, for the SO-CFAR detector, the local power level is estimated by choosing the minimum of the two products of the samples calculated in each of the two semi-windows W_1 and W_2 [12]. The decision rule for the SO-CFAR detector is given by

$$Z_0 \underset{H_0}{\overset{H_1}{\gtrless}} \beta^{1-NT}[min(W_1, W_2)]^T \tag{2.42}$$

where W_1 and W_2 are given by (2.34) and (2.35) respectively.

In this case, the P_{fa} is given simply by

$$P_{fa} = \Pr\left(Z_0 > \beta^{1-NT}\left[min\left(\prod_{i=1}^{N} x_i \,,\, \prod_{i=N+1}^{M} x_i \right) \right]^T \middle| H_0 \right) \tag{2.43}$$

By applying duality (2.18) to the two Pareto distributed random variables Z_0 and x_i(i.e, $Z_0 = \beta e^{\alpha^{-1} Y_0}$ and $x_i = \beta e^{\alpha^{-1} y_i}$) appearing in equation (2.43), and introducing the Napierian logarithmic function, the decision rule (2.42) can then be transformed to the following form corresponding to the Gaussian case:

$$Y_0 \underset{H_0}{\overset{H_1}{\gtrless}} T\, min(U, V) \tag{2.44}$$

where U and V are defined previously.

Note that this transformed rule is identical to that established for the case of a SO-CFAR detector operating in Gaussian noise [10]. We can therefore conclude that the relationship between the P_{fa} and the multiplier T of the Gaussian case is obviously preserved for the Pareto case when applying the logarithmic transformation. Based on (1.13), the P_{fa} of the SO-CFAR detector is given simply by [12]

$$P_{FA} = 2\sum_{r=0}^{N-1} \binom{N+r-1}{r} (2+T)^{-(N+r)} \tag{2.45}$$

Assuming now that the useful signal from the target adds coherently to the Pareto distributed clutter in the CUT, then the P_d is calculated by

$$P_D = \Pr\left(Z_0 > \beta^{1-NT} \left[min\left(\prod_{i=1}^{N} x_i \, , \prod_{i=N+1}^{M} x_i \right) \right]^T \middle| H_1 \right) \qquad (2.46)$$

Similar to the case of the other detectors studied, and as the pdf of $Z_0|H_1$ does not have an analytical form, we then resort to Monte-Carlo simulations to evaluate the P_d.

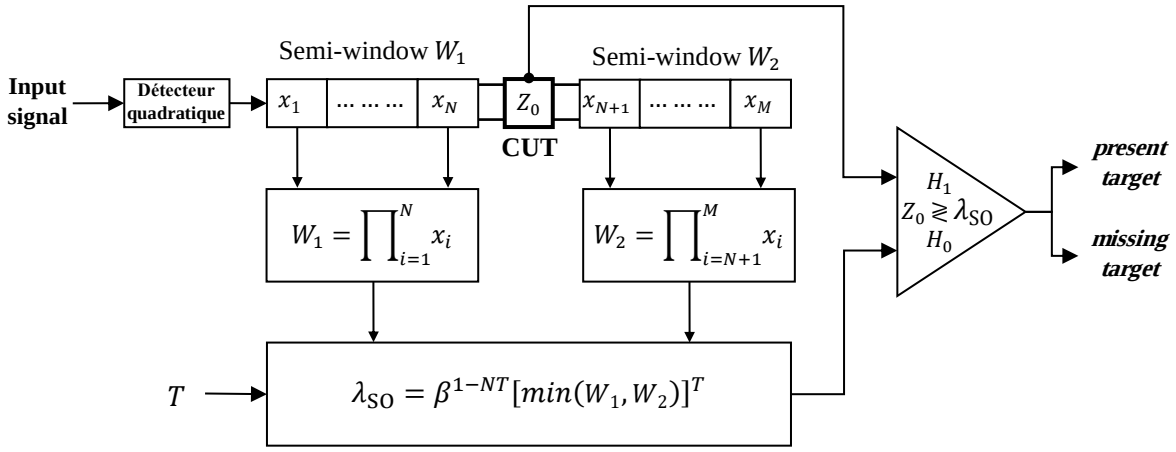

Figure 2.4 - Block diagram of the SO-CFAR detector

2.7 Conclusion

In this second chapter, we provide at the beginning a general overview about CFAR detection of target signal in homogenous Pareto-distributed clutter. The main objective of this chapter is to offer an analytical study of the P_{fa} for three well-known Mean-Level CFAR detectors, namely the GM, ML, GO and SO-CFAR detector. To do so, we present their basic principles, develop their corresponding and propose to compute their corresponding P_d via Monte-Caro simulation. The performance of these detectors will be analyzed and compared in the last chapter.

Chapiter 3 : Simulation Results

3.1 Introduction

In this last chapter, we will test and examine via simulations the discussed CFAR detectors, namely the GM- SO-, GO- and ML-CFAR. First, the different parameters used in our simulations are given. After that, we will validate the proposed expressions of P_{fa} for both detectors, by comparing them to existing integral expressions and to those obtained by simulations, as well. In addition, an approximation of the expression of P_d of the optimal detector is also presented. At the end, the performance of the detectors (i.e, GM, GO, SO and ML-CFAR) is compared against the well-known optimal fixed threshold detector. The former is included here as a benchmark, since it needs a prior knowledge of clutter parameters.

3.2 Simulation parameters

To analyze the performance of the discussed CFAR detectors, we propose to carried out several simulations for various scenarios. The influences of changing different parameters on P_{fa} and P_d, over the detection performance, is also considered for different simulation scenarios.

Due to the lack of analytical expressions for the P_d of these detectors, the detection performance of all detectors has been done using Monte-Carlo (MC) simulation results. The number of trails for MC simulation is 10^6 and the generated observations were considered independent and identically distributed (IID) according to the Pareto-Distribution. To this end, we simulate a Pareto-Distributed clutter by considering $\alpha = 4.7241$ and $\beta = 0.0446$. Both values were chosen because they are drawn from the result of fitting the Pareto-Distribution to a high-resolution X-band grazing angle clutter dataset from the Defense Technology Group Ingara radar [13]. As an exception for the first

experiment, the values of α are taken to be equal to 2.5, 5 and 10. The scale parameter remains equal to 0.0446 in all scenarios.

For each value of α, the size of the reference window for both CFAR detectors is taken to be $M = 16, 32,$ and 48. For each case, the resulted data matrix is of size $M \times 10^6$, so that it can be assimilated to a CFAR reference window, which is generated 10^6 times. Moreover, the content of the CUT is also generated 10^6 times for both hypothesis H_0 and H_1.

In all considered scenarios, the simulated P_{fa} curves were produced using 10^7 Monte-Carlo simulation trials. For each detector, the decision rules (2.12), (2.16), (2.25), (2.33) and (2.42) was also simulated and the corresponding thresholds were estimated accordingly. To study the P_d performance we consider also a Swerling I or II fluctuating target.

3.3 Comparison between ML- CFAR and GM-CFAR

In this section, we examine the performance of ML-CFAR detector against that of GM-CFAR detector. The optimal detector is also included in this comparison. In fact, we study here the effect of changing some parameters on the detection performance of both detectors. Some examples of performance will be analyzed by changing some simulation parameters, namely α, M and the desired P_{fa}.

In the first experiment, the effect of changing shape parameter values is examined and the results are presented on Figure 3.1. In this case, we consider the following several three practical scenarios:

- $\alpha = 2.5$, which means that the clutter is very spiky,
- $\alpha = 5.0$, which means that the clutter is less spiky,
- $\alpha = 10$, which means that the clutter becomes of Gaussian nature,

According to Figure 3.1, it is evident that increasing the value of the shape parameter results in a clear enhancement of the detection performance of both detectors. The degradation of detection quality for $\alpha = 2.5$ is due to the fact that the clutter becomes spikier, which results in an increase of false alarms compared to those predicted for the two other cases where $\alpha = 5.0$ and $\alpha = 10$.

In the second experiment, we study the effect of the reference window length M on the detection performance of both GM and ML detectors. The corresponding results are shown in Figure 3.2. From this figure, we can observe that as M increase, the detection performance improves significantly for both detectors.

On the other hand, the performance of both detectors is highly dependent on the value of the desired false alarm probability α_0 (See Figure 3.3). For $\alpha_0 = 10^{-4}$, the performance loss is quite large compared with the case where $\alpha_0 = 10^{-3}$, but decreases considerably for the other case where $\alpha_0 = 10^{-5}$.

Moreover, it is clear that the ML-CFAR algorithm exhibits minor additional degradation in the detection performance compared to the GM-CFAR detector (See Figures 3.1-3.3). This can be interpreted by the fact that the GM-CFAR is applied assuming that the clutter parameters are known *a priori*. In other words, it uses the exact values of clutter parameters and doesn't need to estimates these parameters. In the other hand, the ML-CFAR is based upon the Maximum Likelihood (ML) estimates of clutter parameters, which results inevitably in some degradation in detection performance. This degradation is even greater as the number of the reference cells M decreases. See for instance the case where $M = 8$ in Figure 3.2. Note that the observations in reference window cells are used in the estimation process of the ML-CFAR. It is well known that

increasing the length of the reference window strongly improves the estimation quality and thus improves also the detection performance.

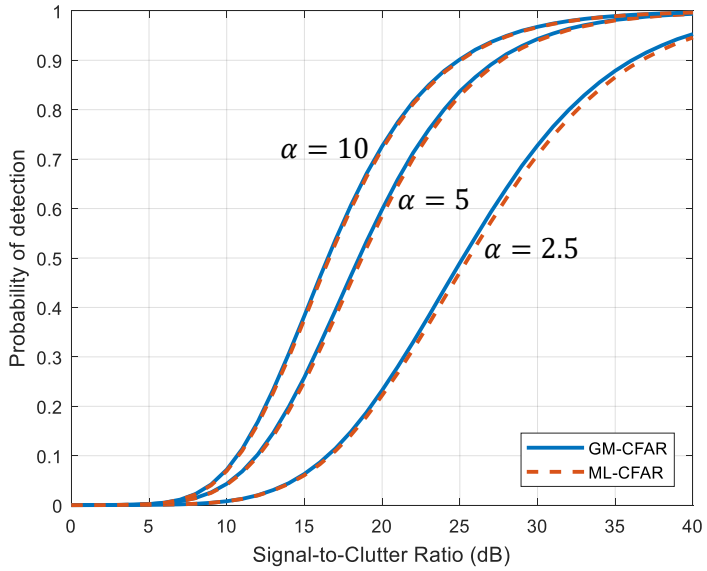

Figure 3.1 - Impact of variation of the value of the shape parameter $\boldsymbol{\alpha}$ on the detection performance of the GM-CFAR and ML-CFAR detectors for $\boldsymbol{M = 16}$ and $\boldsymbol{\alpha_0 = 10^{-4}}$.

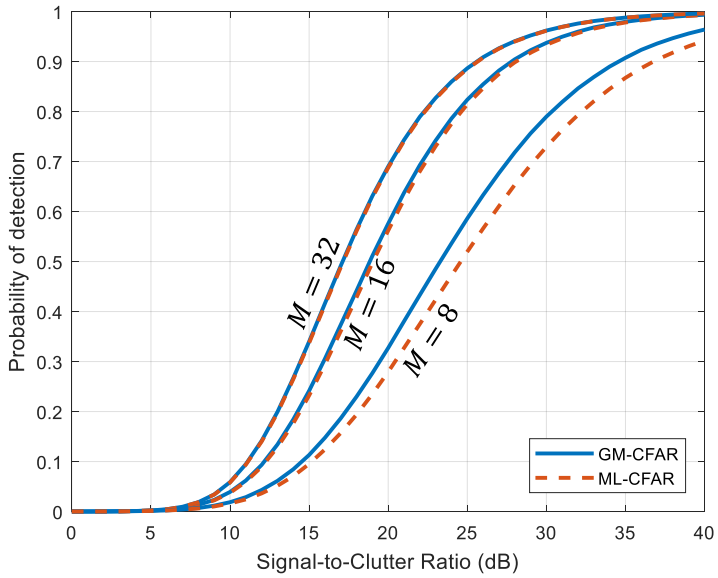

Figure 3.2 - Impact of variation of the length $\boldsymbol{M}$ of the reference window on the detection performance of the GM-CFAR and ML-CFAR detectors for $\boldsymbol{\alpha = 4.7241}$ and $\boldsymbol{\alpha_0 = 10^{-4}}$.

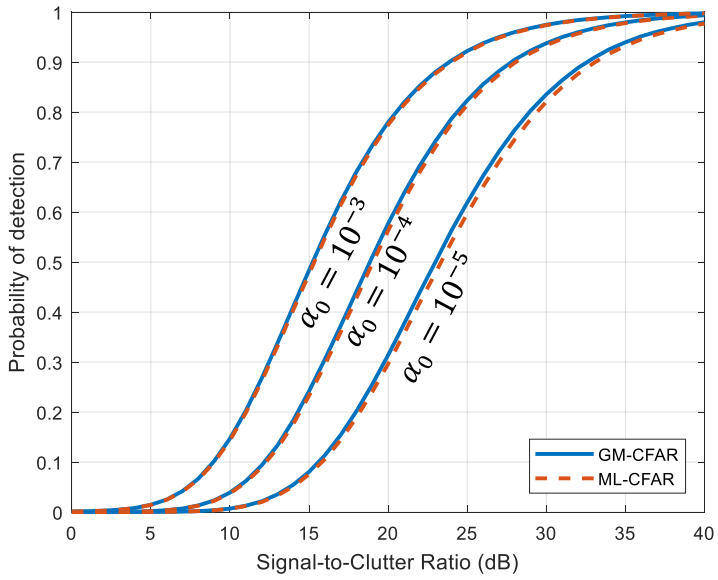

Figure 3.3 - Impact of variation of the desired false alarm probability $\boldsymbol{\alpha_0}$ on the detection performance of the GM-CFAR and ML-CFAR detectors for $\boldsymbol{\alpha = 4.7241}$ and $\boldsymbol{M = 16}$.

3.4 Analysis of detection performance in homogenous backgrounds

Under the assumption of a homogenous clutter, we compare now the detection performance of ML-CFAR to other competitors, namely the GO- and the SO-CFAR detectors. The optimal detector is also included as *a benchmark* in this comparison. The GM-CFAR detector is omitted in this comparison. The results are presented on Figure 3.4 for the case where $M = 32$ and on Figure 3.5 for the case where $M = 16$.

In both figures, we can see that the performance of the ML-CFAR detector is closest to that of the Optimal detector, compared with the GO and SO-CFAR detectors. Moreover, the performance of GO-CFAR is slightly better than that of the SO-CFAR. The detection losses of all the three detectors are even greater compared with the Optimal detector for $M = 16$ (See Figure 3.5). For $P_d = 0.5$, the detection loss of the ML-CFAR detector is around 3dB relative to the Optimal detector according to this last figure. Moreover, the additional detectability loss introduced by GO-CFAR detector is very

small relative to the ML-CFAR and is around 4dB relative to the Optimal case. In the case of the SO-CFAR detector the additional detectability loss is shown to be important approximately 7dB.

However, the detection losses as compared to the case with $M = 32$ (Figure 3.4) are significantly decreased for all considered detectors due to the enhanced performance offered by increasing the size of the reference window. In this case, it is evident that the ML-CFAR still provides the best performance compared to the GO- and SO-CFAR detector.

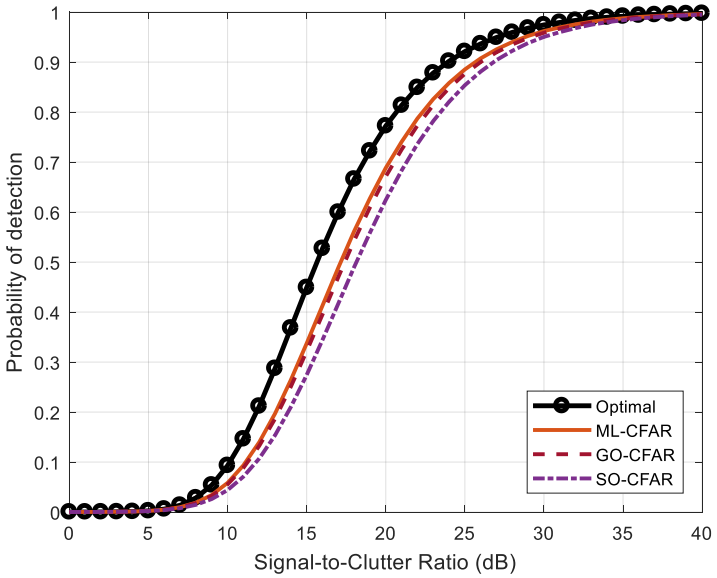

Figure 3.4 - Probability of Detection of Optimal, ML-CFAR, GO-CFAR and SO-CFAR detectors for $\boldsymbol{\alpha = 4.7241}$, $\boldsymbol{M = 32}$ and $\boldsymbol{\alpha_0 = 10^{-4}}$.

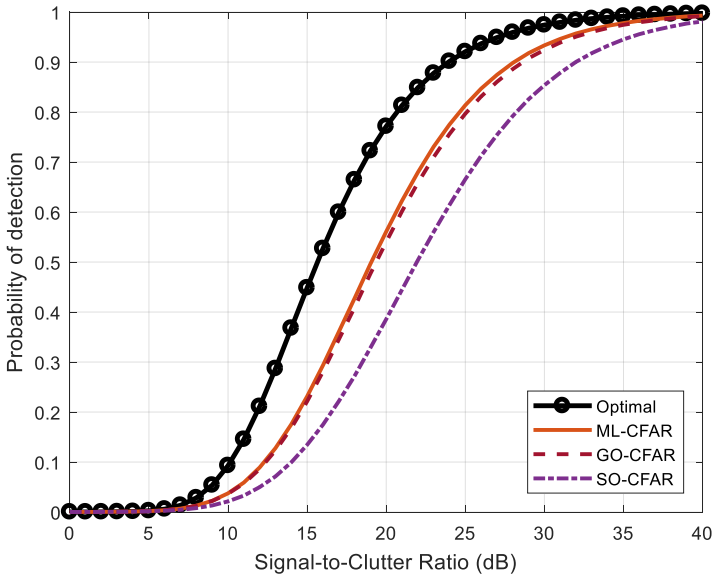

Figure 3.5 - Probability of Detection of Optimal, ML-CFAR, GO-CFAR and SO-CFAR detectors for $\boldsymbol{\alpha = 4.7241}$, $\boldsymbol{M = 16}$ and $\boldsymbol{\alpha_0 = 10^{-4}}$.

3.5 Analysis of detection performance in heterogenous backgrounds

In this section, we will compare the detection performance of ML-CFAR, GO-CFAR and SO-CFAR processors, by assuming the case of heterogenous Pareto-Distributed clutter. The heterogeneity is caused here by assuming the presence of single, two and/or three interfering targets in the reference window of a given CFAR detector.

3.5.1 Case 1: Presence of a single interfering target

At the beginning, we analyze, through Figure 3.6 ($M = 16$) and Figure 3.7 ($M = 32$), the detection performances of Optimal, ML-CFAR, GO-CFAR and SO-CFAR detectors for an ICR (Interference-to-Clutter Ratio) equal to 20dB. After that, we study, in Figure 3.8 ($M = 16$) and Figure 3.9 ($M = 32$), the performance of the same algorithms for a $ICR = 40$dB.

The first observation, illustrated by both Figures 3.6 and 3.7, is that the performance of the SO-CFAR detector is better that that of the ML and GO-CFAR detectors. Both the ML and GO-CFAR detectors suffer from the capture effect since the interfering target in the reference window of the primary target raises the adaptive threshold. As depicted in Figure 3.6, the performance of these two detection algorithms is more degraded, because the capture effect is very important for the case where $M = 16$. The ML-CFAR detector, on the other hand, shows a certain loss compared with the SO-CFAR detector. We note that the performance of the GO-CFAR detector is the worst.

Moreover, it is clear that the performance of the SO-CFAR detector remains unchanged when the ICR increases from 20dB to 40dB (see for instance both Figure 3.7 and 3.8). For the same situation, we also note the remarkable degradation in performance of the ML-CFAR and GO-CFAR detectors if the value of ICR changes from 20dB to 40dB. This is explained by the fact that both ML- CFAR and GO-CFAR detectors both suffer from the capture effect caused by the presence of interfering targets in the detection background.

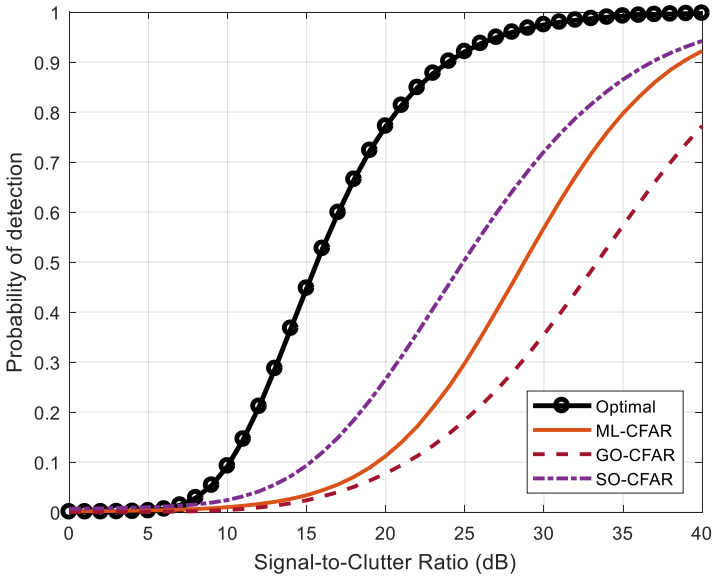

Figure 3.6 – Probability of Detection of Optimal, ML-CFAR, GO-CFAR and SO-CFAR detectors in presence of a single interfering target with $\boldsymbol{ICR = 20dB}$ for $\boldsymbol{\alpha = 4.7241}$, $\boldsymbol{\alpha_0 = 10^{-4}}$ and $\boldsymbol{M = 16}$.

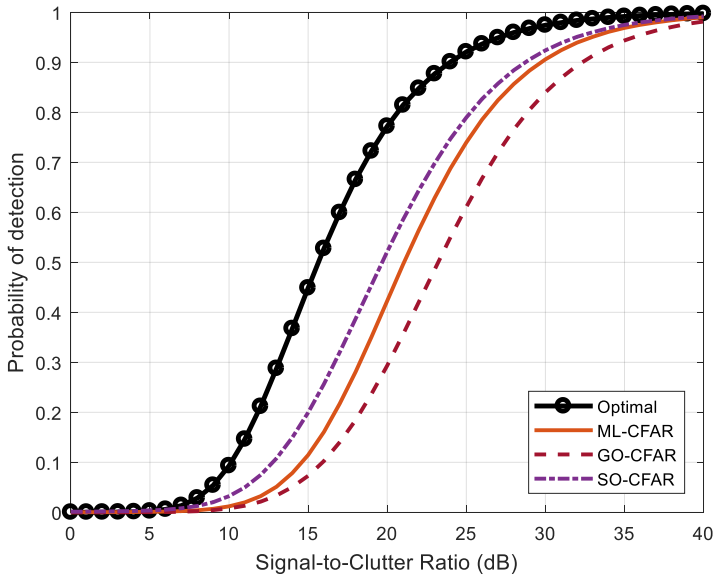

Figure 3.7 – Probability of Detection of Optimal, ML-CFAR, GO-CFAR and SO-CFAR detectors in presence of a single interfering target with $\boldsymbol{ICR = 20dB}$ for $\boldsymbol{\alpha = 4.7241}$, $\boldsymbol{\alpha_0 = 10^{-4}}$ and $\boldsymbol{M = 32}$.

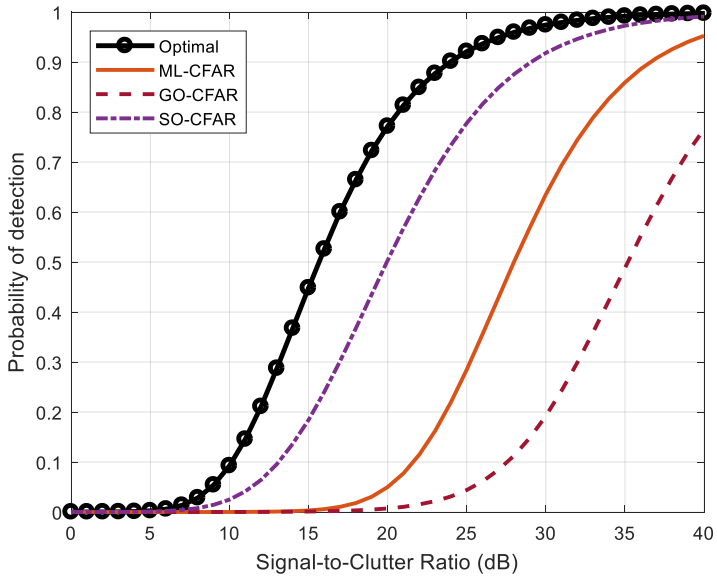

Figure 3.8 – Probability of Detection of Optimal, ML-CFAR, GO-CFAR and SO-CFAR detectors in presence of a single interfering target with $\boldsymbol{ICR = 40dB}$ for $\boldsymbol{\alpha = 4.7241}$, $\boldsymbol{\alpha_0 = 10^{-4}}$ and $\boldsymbol{M = 32}$.

3.5.2 Case 2: Presence of more than one interfering targets

Now, we study the impact of presence of more than one interfering target in the reference window. According to their positions, two possible scenarios are likely to be encountered in practical situations:

- Both extraneous targets are located in one-half reference window;
- One extraneous target is located in the leading half window, but the second one is located in lagging half window.

For the first scenario, which is studied in Figure 3.9, it can be seen from these results that the SO-CFAR processor is capable of resolving the presence of multiple interfering targets in the reference window as long as all the interferers appear either in the leading or lagging window.

For the second scenario where two interfering targets are present, one in the leading and the other in the lagging half reference window, the detection performance of all three detectors, including the SO-CFAR, is seriously degraded due to the capture effect (See Figure 3.10). Although the SO-CFAR scheme is preferrable in presence of extraneous targets, its performance degrades significantly also. This is because it suffers from the capture effect if the interfering targets are located separately in both halves of the reference window. For both scenarios, the degradation of performance associated with the ML-CFAR and the GO-CFAR detectors is more severe.

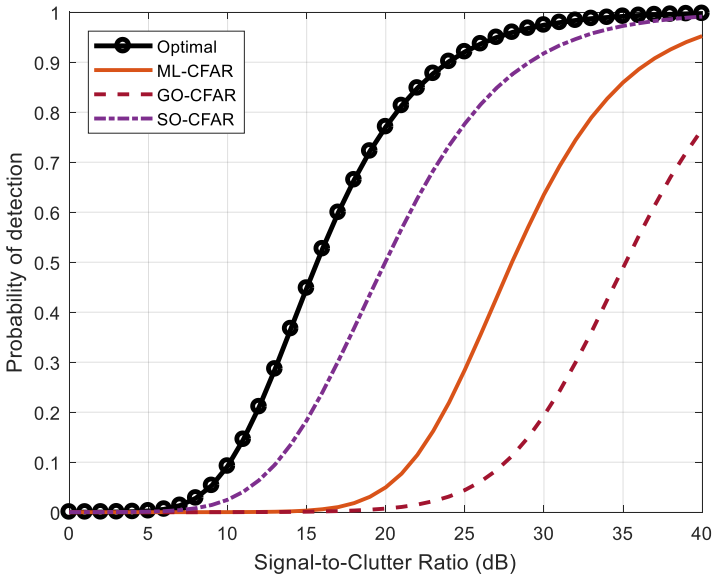

Figure 3.9 – Probability of Detection of Optimal, ML-CFAR, GO-CFAR and SO-CFAR detectors in presence of two interfering targets both located in one-half reference window with $\boldsymbol{ICR_1 = 20dB}$, $\boldsymbol{ICR_2 = 40dB}$, $\boldsymbol{\alpha = 4.7241}$, $\boldsymbol{\alpha_0 = 10^{-4}}$ and $\boldsymbol{M = 32}$.

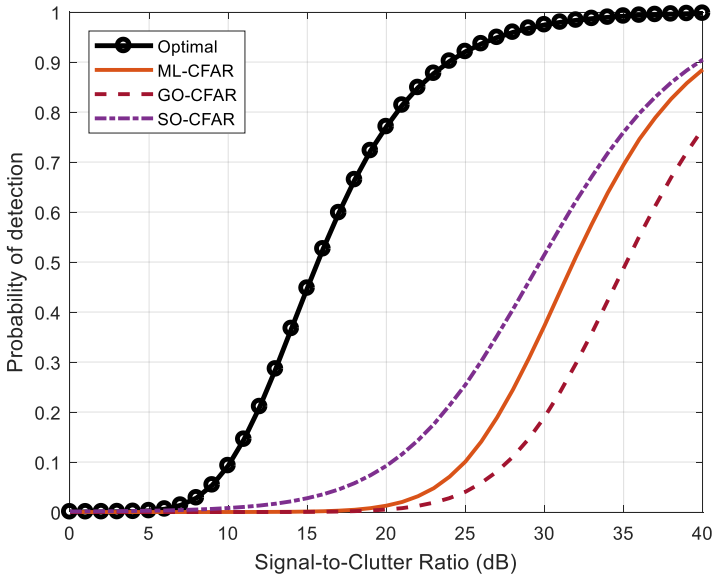

Figure 3.10 – Probability of Detection of Optimal, ML-CFAR, GO-CFAR and SO-CFAR detectors with one interfering target in each half of the reference window with $\boldsymbol{ICR_1 = 20dB}$, $\boldsymbol{ICR_2 = 40dB}$, $\boldsymbol{\alpha = 4.7241}$, $\boldsymbol{\alpha_0 = 10^{-4}}$ and $\boldsymbol{M = 32}$.

3.5 Conclusion

In this chapter, we first compared the detection performance of the ML-CFAR detector against that of the GM-CFAR algorithm by varying the shape parameter of the Pareto-Distribution, the length of the reference window and the desired false alarm probability. After that, performance analysis of the ML-CFAR processor in homogenous background was also examined against those of the Optimal, GO-CFAR and SO-CFAR detectors. Finally, we tested these three detectors (i,e; Optimal, ML, GO and SO) over heterogeneous backgrounds by considering the presence of single and/or two interfering targets. From to the obtained results, we conclude that the ML-CFAR detector is well suited for homogenous backgrounds, while the SO-CFAR detector is relatively efficient against interfering targets.

Conclusion and perspectives

▪ *Conclusion*

This dissertation addresses the problem of CFAR detection of targets embedded in a non-Pareto-Distributed clutter. This research issue is of great importance and falls within the general framework of radar signal processing. In general, we analyzed the detection performance of some CFAR processors, namely ML-CFAR, GM-CFAR, GO-CFAR and SO-CFAR detectors, by considering several scenarios.

In fact, the study conducted here covers two types of cluttered backgrounds: homogeneous and heterogeneous. In both cases, we provided a theoretical analysis on the above-mentioned CFAR detectors and highlight their advantages and disadvantages. Moreover, we demonstrated the full CFAR property of the ML-CFAR detector, and showing that it does not require any prior knowledge about clutter distribution parameters.

After that, the performances of all discussed detectors are illustrated via numerical simulations and thus compared in parallel with those of the optimal detector. We have also shown the efficiency of the ML-CFAR detector for homogenous backgrounds and shown that the SO-CFAR detector offers good detection performance in the presence of interfering targets.

▪ *Perspectives*

The issues addressed in this dissertation are certainly very wide, and therefore far from being fully covered in a single manuscript. Thus, in addition to the promising results presented here, the following perspectives can be envisaged in future works:

- ✓ The analysis of CFAR detection performance in the presence of clutter transitions (or discontinuities) will be an important topic for further discussion.
- ✓ It would also be interesting to analyze and examine the ML-CFAR, SO-CFAR and GO.
- ✓ It is also worth considering the realistic case where the clutter parameters are completely unknown a priori. This will contribute enormously to improving detection performance in non-Gaussian environments.

References

[1] M. Skolnik, Introduction to Radar System, (3rd ed.), New York: McGraw-Hill Education, 2001.

[2] M. Sahed, Radar Systems, Course material, M'Sila: University of M'Sila, 2022.

[3] G. Weinberg, "Assessing the Pareto fit to high resolution high grazing angle sea clutter," *Electronics Letters*, vol. 47, no. 8, pp. 516-517, Apr. 2011.

[4] G. V. Weinberg, "An investigation of the Pareto distribution as a model for high grazing angle clutter," Defense Science and Technology Organization, Edinburgh, Australia, 2011.

[5] C. D. Schleher, "Radar detection in Weibull clutter," *IEEE Transactions on Aerospace and Electronic Systems*, vol. 12, no. 6, pp. 736-743, 1976.

[6] M. Sahed, E. Kenane, A. Khalfa and F. Djahli, "Exact Closed-Form Pfa Expressions for CA- and GO-CFAR Detectors in Gamma-Distributed Radar Clutter," *IEEE Transactions on Aerospace and Electronic Systems*, vol. 59, no. 4, pp. 4674 - 4679, Aug. 2023.

[7] M. Sahed, E. Kenane, A. Khalfa and F. Djahli, "Performance Analysis of the MLG-CFAR Detector in Homogenous Gamma-Distributed Sea Clutter," *IEEE Geoscience and Remote Sensing Letters*, vol. 20, pp. 1-5, Sep. 2023 (Art no. 3506905, doi: 10.1109/LGRS.2023.3303225.).

[8] S. Watts, "Radar detection prediction in sea clutter using the compound K distribution model," *IEE Proceedings*, vol. 132, no. 7, pp. 613-620, 1985.

[9] G. V. Weinberg, "Constant False Alarm Rate Detectors for Pareto Clutter Models," *IET Radar, Sonar and Navigation*, vol. 7, no. 2, pp. 153-163, Feb. 2013.

[10] P. P. Gandhi and S. A. Kassam, "Analysis of CFAR processors in nonhomogeneous background," *IEEE Transactions on Aerospace and Electronic Systems*, vol. 24, no. 4, pp. 427-445, 1988.

[11] V. G. Hansen, "Constant false alarm rate processing in search radars," in *Proceedings of the IEEE International Radar Conference*, London, 1973.

[12] G. V. Weinberg, "Constant false alarm rate detection in Pareto distributed clutter: Further results and optimality issues," *Contemporary Engineering Sciences*, vol. 7, no. 6, pp. 231-261, 2014.

[13] G. V. Weinberg, "On the Construction of CFAR Decision Rules via Transformations," *IEEE Transactions on Geoscience and Remote Sensing*, vol. 55, no. 2, pp. 1140-1146, 2017.

[14] G. V. Weinberg., "Management of interference in Pareto CFAR processes using adaptive test cell analysis," *Signal Processing*, vol. 104, pp. 264-273, 2014.

[15] M. Sahed and A. Mezache, "Analysis of CFAR Detection with Multiple Pulses Transmission Case in Pareto Distributed Clutte," in *4th International Conference on Electrical Engineering*, Algérie, boumerdès, 2015.

[16] R. Benhamed and S. Bounif, *Étude et Analyse des Détecteurs Adaptatifs CFAR de Cibles Radar Noyées dans un Milieu Non Gaussien*, M'Sila: University of M'Sila, 2022.

[17] A. M'hamdi and M. Chabani, *Performance du détecteur GM-CFAR avec intégration non-cohérente en milieux côtiers Pareto distribués*, M'Sila: University of M'Sila, 2021.

[18] M. Sahed, *Détection Automatique CFAR en environnement Non Gaussien, Thèse de Doctorat ès science*, M'Sila: University of M'Sila, 2015.

[19] A. L. Prastitis, *On adaptive censored CFAR detection, PhD dissertation*, New Jersey: New Jersey Institute of Technology, 1993.

[20] K. Krishnamoorthy, Handbook of Statistical Distributions with Applications, USA: Chapman & Hall/CRC, 2006.

[21] M. Barkat, Signal Detection and Estimation, London: Library of Congress Cataloging in Publication Data, 2005.

[22] H. M. Finn and R. S. Johnson, "Adaptive detection mode with threshold control as a function of spatially sampled clutter level estimates," *RCA Review*, vol. 29, no. 3, p. 414–464, Sept. 1968.

[23] G. Minkler and J. Minkler, CFAR – the principles of automatic radar detection in clutter, Baltimore: Magellan, 1990.

[24] F. Gini, F. Lombardini and L. Verrazzani, "Decentralized CFAR detection with binary integration in Weibull clutter," *IEEE Transactions on Aerospace and Electronic Systems*, vol. 33, no. 2, pp. 396-407, Apr. 1997.

[25] R. Ravid and N. Levanon, "Maximum-likelihood CFAR for Weibull background," *IEE Proc. F Radar Signal Process*, vol. 139, no. 3, p. 256–264, Jun. 1992.

***Abstract* —** In this study, we address the problem of adaptive detection of embedded radar targets in a Pareto distributed clutter. This type of detection is achieved by maintaining a constant false positive rate (CFR) during processing. We first introduce the geometric mean CFAR (GM-CFAR) detector introduced in the literature. The detector is suitable for homogeneous clutter. We show that the derivation of this detector is obtained by exploiting the duality between both exponential and Pareto distributions. This duality makes it possible to convert CFAR detection strategies developed for Gaussian noise into Pareto distributed clutter. In addition, we have presented a modified version of the GM-CFAR, which is called the Maximum Likelihood (ML) CFAR detector, and thus give the corresponding analytical expression of the false alarm probability. For comparison purposes, we perform as well a partial theoretical analysis of two other detectors, namely the Greatest Of (GO) CFAR and the Smallest Of (SO) CFAR algorithms. Via numerical simulations, the performance of the ML-CFAR scheme has been compared and examined against those of the Optimal, GM, GO and SO-CFAR detectors. The simulation results obtained validate the interest of the ML-CAFR detector in homogenous backgrounds, but shows that its performance degrades in heterogenous backgrounds. Moreover, it has been also shown from these results that the SO-CFAR detector is relatively efficient against interfering targets.

Keywords: Radar CFAR detection, non-Gaussian clutter, Pareto-Distribution, Maximum Likelihood Estimates, ML-CFAR, GM-CFAR, GO-CFAR, SO-CFAR.

ملخص — ناقشنا من خلال هذه الدراسة مسألة الكشف عن الأهداف المهمة المتواجدة في وسط (محيط) متجانس وغير متجانس، بحيث تكون الاشارات العشوائية (clutter) الناتجة عن هذا الوسط موزعةً توزيعًا احصائيًا غير طبيعيٍ حسب نموذج باريتو (Pareto model). قمنا باستعمال تقنية الكشف التكيفي بنسبة إنذار خاطئ ثابتة (CFAR Detection)، باعتبارها وسيلة ناجعة في مثل هذه الأوساط سريعة التغير. في البداية، أجرينا دراسةً تحليليةً كاملةً للكاشف المعروف GM-CFAR بناءً على نموذج باريتو، والذي تم اقتراحه في أبحاث سابقة وهو كاشف مخصص للأوساط المتجانسة. هذا الأخير يعتمد على المتوسط الهندسي للعينات المتواجدة داخل النافذة المرجعية للكاشف (Reference Window) لحساب عتبة الكشف. حيث بيَّنا أن تصميم هذا الكاشف يتم باستخدام العلاقة التحويلية بين دالة كثافة الاحتمال الأسي وقانون باريتو الاحصائي. بحيث تسمح لنا هذه العلاقة بتحويل خوارزميات الكشف المصممة خصيصًا للوسائط الغاوسية الطبيعية ذات توزيع احتمالي أسي،للعمل مع الوسائط الغير الطبيعية ذات توزيع احتمالي حسب نموذج باريتو. بعد ذلك، قمنا ببعض التغييرات على الكاشف GM-CFAR لنتحصل على نسخة عملية، سميناها الكاشف ML-CFAR الذي يعتمد على طريقة تقدير الأرجحية القصوى (Maximum Likelihood Estimates) في حساب العتبة، دون الحاجة لمعلومات مسبقة عن معالم الاشارات العشوائية الغير الطبيعية. باستعمال نفس علاقة التحويل، قمنا بعد ذلك بدراسة نظرية وتحليلة للكاشفين GO-CFAR و SO-CFAR. هذا الأخير تم اقتراحه خصيصا للأوساط الغير متجانسة التي تحتوي على أهداف دخيلة. من خلال عمليات المحاكاة الرقمية، قمنا بمقارنة واختبار أداء مختلف الكاشفات التي تمت دراستها ومناقشتها في هذا العمل. حيث أكدت النتائج المتحصل عليها على نجاعة الكاشف ML-CFAR في الأوساط المتجانسة وكذا فعالية SO-CFAR في حالة وجود أهداف دخيلة مقارنة بالكاشفات الأخرى.

الكلمات المفتاحية: الرادار، الكشف المكيف بنسبة إنذار خاطئ ثابتة، التشويش الغير غاوسي(الغير طبيعي)، توزيع باريتو، تقدير الأرجحية القصوى ML-CFAR، GM-CFAR، SO-CFAR، GO-CFAR.